THESIS
C.1

MICHIGAN STATE UNIVERSITY LIBRARIES
3 1293 00896 9689

This is to certify that the

thesis entitled
The Application of Fiber Optics
as a Light Delivery or Imaging System
For Flow Studies Using High Power Lasers

presented by
Lorna J. Clowater

has been accepted towards fulfillment
of the requirements for

M.S. degree in Mech. Engineering

Harold G. Schock
Major professor

Date 9/21/91

O-7639 *MSU is an Affirmative Action/Equal Opportunity Institution*

LIBRARY
Michigan State
University

PLACE IN RETURN BOX to remove this checkout from your record.
TO AVOID FINES return on or before date due.

DATE DUE	DATE DUE	DATE DUE

MSU Is An Affirmative Action/Equal Opportunity Institution
c:\circ\datedue.pm3-p.1

APPLICATIONS OF FIBER OPTICS AS LIGHT DELIVERY OR IMAGING SYSTEMS FOR FLOW STUDIES USING HIGH POWER LASERS

By

Lorna J. Clowater

A THESIS

Submitted to
Michigan State University
in partial fulfillment of requirements
for the degree of

MASTERS OF SCIENCE

Department of Mechanical Engineering

1991

80-5887

ABSTRACT

APPLICATIONS OF FIBER OPTICS AS LIGHT DELIVERY OR IMAGING SYSTEMS FOR FLOW STUDIES USING HIGH POWER LASERS

By

Lorna J. Clowater

The purpose of this study was to develop a fiber optic light delivery and imaging system for flow quantification studies using high power laser light.

A fused fiber optic bundle with collimating GRIN lenses mounted to the ends of the fibers was used to enhance light delivery techniques which require collimated light beams for fluid analysis. To enhance imaging techniques, a flexible fiber optic image carrier was coupled with a high speed camera to create a unique imaging system which can easily reach remote location test sites.

The fused fiber bundle with the collimating lenses did not collimate the emitting light from the fibers as well as expected, and therefore this light delivery system was not pursued further. However, the image carrier did prove to be a useful tool for viewing remote flow fields and successful flow visualization tests were conducted in internal combustion engines.

ACKNOWLEDGMENTS

I would like to express my gratitude and appreciation to several people whose guidance and support made this work possible. I would first like to thank my advisor Dr. H. Schock for letting me pursue a subject I was interested in. His technical guidance and support was invaluable and very much appreciated; to Dr. C. Somerton and Dr. E. Scott, the other committee members for their time and supportive comments. I would like to acknowledge Dr. F. Hamady whose patience and expertise with the flow visualization technique allowed the success of this project, and I would also like to thank K. Zimmerman for her technical comments and tireless editing.

I must also express my appreciation to NASA Lewis Research Center and Chrysler Corporation for their support of this project.

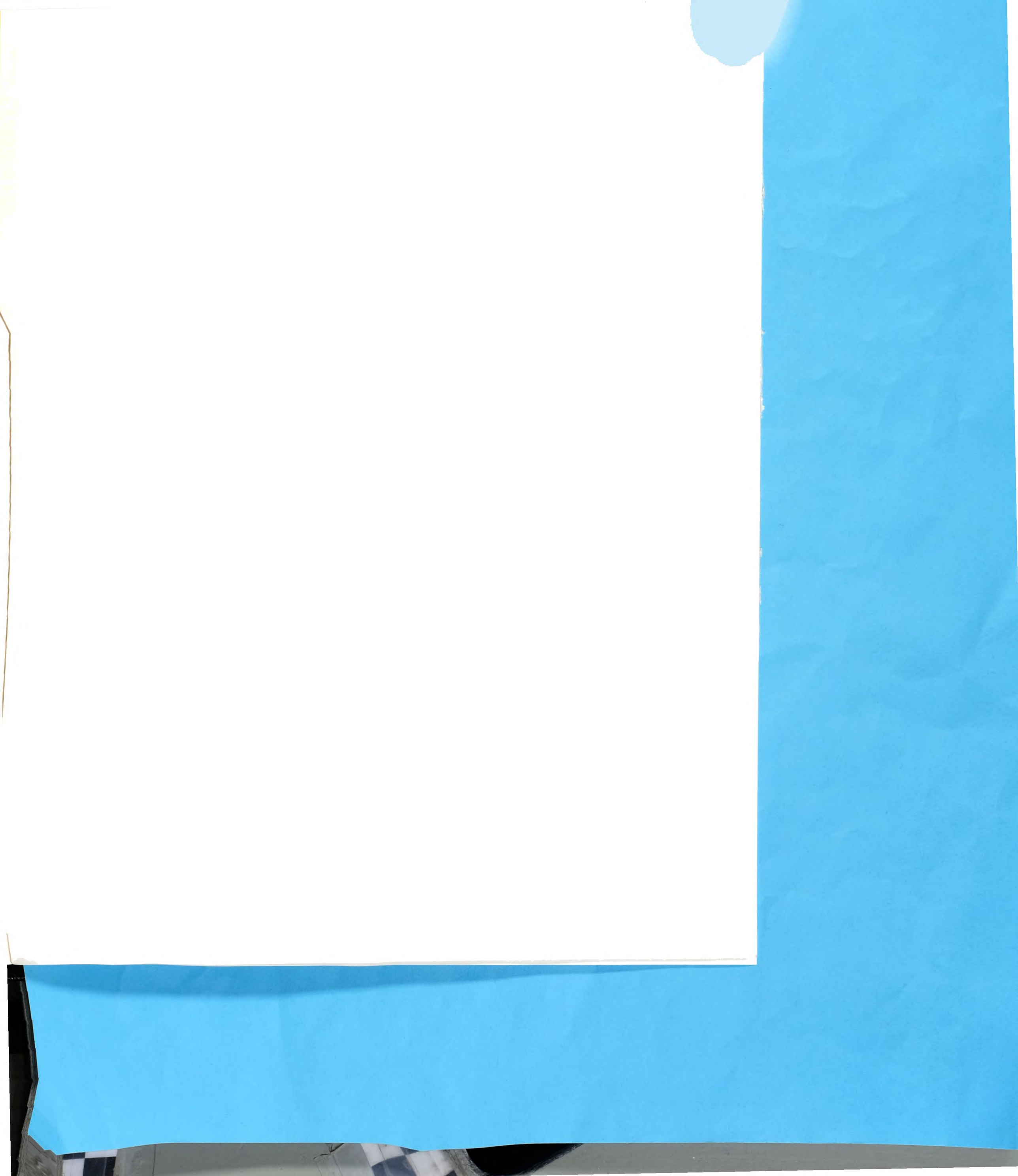

TABLE OF CONTENTS

Page

LIST OF TABLES vii

LIST OF FIGURES viii

LIST OF SYMBOLS ix

CHAPTER 1 - INTRODUCTION

1.1 Current Work and Research Motivation 1

1.2 Background 3

1.3 Fiber Optics 5

CHAPTER 2 - FIBER OPTIC APPLICATIONS TO FLUID QUANTIFICATION METHODS 15

2.1 Light Delivery Systems 15

A. Light Input 15

B. Light Output 18

(1). Flow Visualization Using Fiber Optics 19

(2). Particle Image Velocimetry (PIV) 22

(3). Laser Induced Photochemical Anemometry 24

2.2 The Fused Fiber Bundle and its Application to LIPA 27

A. Description of a Fiber Bundle 27

B. Assembly of a GRIN Lens Collimator 31

C. Performance of the Bundle 33

2.3 Imaging 37

CHAPTER 3 - TESTING APPLICATIONS IN INTERNAL COMBUSTION ENGINES 44

3.1 Testing in a Rotary Engine 44

3.2 Testing in a Mass Air Flow Sensor 47

3.3 Flow Visualization in a Steady State Cylinder Head 50

3.4 Flow Visualization in a Motored Engine 52

CHAPTER 4 - SUMMARY AND CONCLUSIONS 59

CHAPTER 5 - RECOMMENDATIONS 62

APPENDIX A - The Microballoon Seeder 64

APPENDIX B - Microballoon Concentrations for Different Flow Rates 68

LIST OF REFERENCES 71

LIST OF TABLES

Page

Table 1 Range of Values for Common Optical Fibers..... 14

LIST OF FIGURES

P

Figure 1.1 Schematic of a fiber optic..... 6

Figure 1.2 Reflected rays between the fiber core and cladding..... 8

Figure 1.3 Different light propagation in fibers (a) multimode step-index, (b) multimode graded-index and (c) single mode step-index fiber..... 10

Figure 1.4 Optical fibers acceptance cone for incoming light..... 11

Figure 2.1 Light entering a fiber outside the acceptance cone.....16

Figure 2.2 Input end of a typical fiber bundle.....17

Figure 2.3 Light delivery and imaging in a flow visualization system..... 20

Figure 2.4 Fiber optics in flow visualization..... 22

Figure 2.5 Optical arrangement for the LIPA technique using a) stepper mirrors and b) fiber optics.....26

Figure 2.6 Fused fiber bundle for high power laser coupling.....28

Figure 2.7 Front input face of fused fiber bundle..... 28

Figure 2.8 GRIN lens with continuously changing index of refraction..... 30

Figure 2.9 Schematic of an M-type collimator..... 30

Figure 2.10 GRIN lens assembly with a) the fiber in the ferrule b) the front input face showing the off-center alignment of the fiber in the ferrule..... 32

Figure 2.11 The entire input face of the bundle illuminated from light entering one fiber at the output end of the bundle..... 35

Figure 2.12 Image transmission through a flexible image carrier.....38

Figure 2.13 Olympus flexible image carrier..... 40

Figure 2.14 Spatial resolution versus bundle diameter for a 1 cm object..... 43

Figure 3.1 Flow visualization using transport windows for optical imaging..... 45

Figure 3.2 Flow visualization using the image carrier for optical imaging.....45

Figure 3.3 Polar diagram illustrating the relative intensity magnitudes from

particle scatter on different size particles..... 47

Figure 3.4 Air duct assemble and test configuration..... 48

Figure 3.5 Successive frames illustrating Mie scattering angles in an air duct assembly..... 49

Figure 3.6 Schematic showing the experimental setup for flow visualization in the steady state 2.2L cylinder head..... 51

Figure 3.7 Spark plug holder for the image carrier..... 52

Figure 3.8 Motored engine experimental setup..... 54

Figure 3.9 Successive frames from the motored engine using the 80 degree FOV and the mc-08 camera adaptor. (exposure time of 20 ns)..... 56

Figure 3.10 Successive frames from the motored engine using the 80 degree FOV and the mc-05 camera adaptor. (exposure time of 20 ns)..... 57

Figure 3.11 Successive frames from the motored engine using the 40 degree FOV and the mc-05 camera adaptor. (exposure time of 20 ns)..... 58

LIST OF SYMBOLS

C_n speed of light in a medium (km/s)

c speed of light in free space (km/s)

n index of refraction of a material

n_1 index of refraction of the fiber core

θ_2 incident angle to the normal of the core/cladding interface (radians)

n_2 index of refraction of the fiber cladding

θ_R refracted angle to the normal of the core/cladding interface (radians)

θ_c critical angle of incidence at core/cladding interface (radians)

NA numerical aperture for a fiber

θ half angle of the acceptance cone of the fiber

P(L) output power of the fiber

P(0) optical power into the fiber

α attenuation coefficient of the fiber

L length of the fiber

d fiber core diameter

M magnification factor of a fiber bundle

CHAPTER 1

INTRODUCTION

1.1 Current Work and Research Motivation

The characterization of flow fields using laser diagnostic methods is extremely important to the understanding of engine fluid mechanics. The use of laser light provides a unique approach to fluid analysis because it allows for the non-intrusive measurement of flow fields. At Michigan State University's Engine Research Laboratory (MSUERL), flow quantification studies with lasers are being conducted on a number of different projects. The objective of this thesis is to quantify fluid flow in internal combustion engines to better understand the fundamentals of the combustion process and hence control emissions with increased engine efficiency.

The general approach to quantifying these internal flows is to bring the laser light into the engine through a transparent window. The flow in the engine is seeded with either smoke, microballoons or phosphorescing particles. The particle trajectory is assumed to represent the features of the flow field. As the laser light scatters off each particle a real time imaging of the flow field is created. This image is then recorded onto a photographic film.

There are a number of different techniques that use the general approach described above to quantify fluid flow such as, Laser Induced Photochemical Anemometry (LIPA) [1], Particle Image Velocimetry (PIV) [2] and Flow Visualization [3]. These methods will be discussed in greater detail in chapter 2. These techniques all require a light source to illuminate the flow field and a high speed film camera or CCD (charged coupled device) photodiode array to record microscopic motions occurring in the flow field. Frequently a pulsed laser is used as this light source. Currently, conventional optics,

such as lenses and mirrors, are used to deliver light into the engine. The light enters the engine through a transparent window and the flow field is visualized through another window positioned at 90 degrees to the previous window. This allows for perpendicular viewing of the plane of motion. However, conventional optics and large optical access windows have disadvantages. A listing of the disadvantages of both conventional optics and transparent windows is outlined below.

Limitations in the use of conventional optics:

1. Both lenses and optical windows exhibit refraction (bending of light) and light loss due to the reflection of laser light off each of the optical surfaces.

2. Lenses may produce aberrations, which are imperfections of the image, or the inability to focus all the light at the correct focal point of the lens.

3. The use of lenses, mirrors, and windows in an optical imaging setup requires direct (light beam) access to the part being studied. Therefore, the ability to optically interrogate remote areas is greatly inhibited.

Limitations in the use of transparent window:

1. Windows are expensive in terms of materials and assembly time.

2. For internal flow experiments, such as in engines, windows must exhibit sufficient mechanical properties frequently at high temperatures while maintaining optical clarity.

3. There may be difficulty in maintaining a " leak-proof " seal at the window/housing interface.

4. The alignment of the window in the engine housing is critical to prevent interference with the flow field.

The implementation of optical fibers could play an important role in the design of a light delivery and imaging system used for engine fluid flow research. The fiber optic

system would be designed to replace the conventional optics and access windows used to perform the study. The important advantages of fiber optics to engine studies is in light delivery to the engine and in the imaging of the flow field.

Both light delivery and imaging using fiber optics is currently used with Laser Doppler Velocimetry (LDV) [4] . For the LDV technique, a low power continuous wave laser is used and coupled into the fiber optic. This low power light is not high enough to burn the fibers, however it is capable of delivering sufficient light to the system. LDV is a method that measures singular velocities at particular points of interest. Therefore, the studies in this paper will go one step further and will concentrate on planar motion in the flow field in order to quantify velocity gradients in a given plane of interest. To study these planar motion flow fields, most techniques require larger laser power densities. This larger power is achieved by using high powered pulsed lasers. When these more powerful lasers are coupled into fiber optics, the coupling technique becomes critical because the individual fibers tend to burn from the intense energy of the laser.

This study will also address the benefits of developing a fiber optic system for flow field analysis and visualization, as well as the feasibility of such a system. Therefore, the goal of this study is to provide a reference for future designs of light delivery and imaging systems in engine studies. This will be done by exploring the benefits and limitations of fiber optics.

1.2 Background

Over the past twenty years, there has been considerable growth in the use of fiber optics as a research tool. Fibers have been used in everything from communication systems to the creation of a hologram. However, very little work has been done with fiber optics in engine studies, especially when high powered lasers are incorporated. In the two areas of interest, light delivery and imaging, an extensive literature analysis was

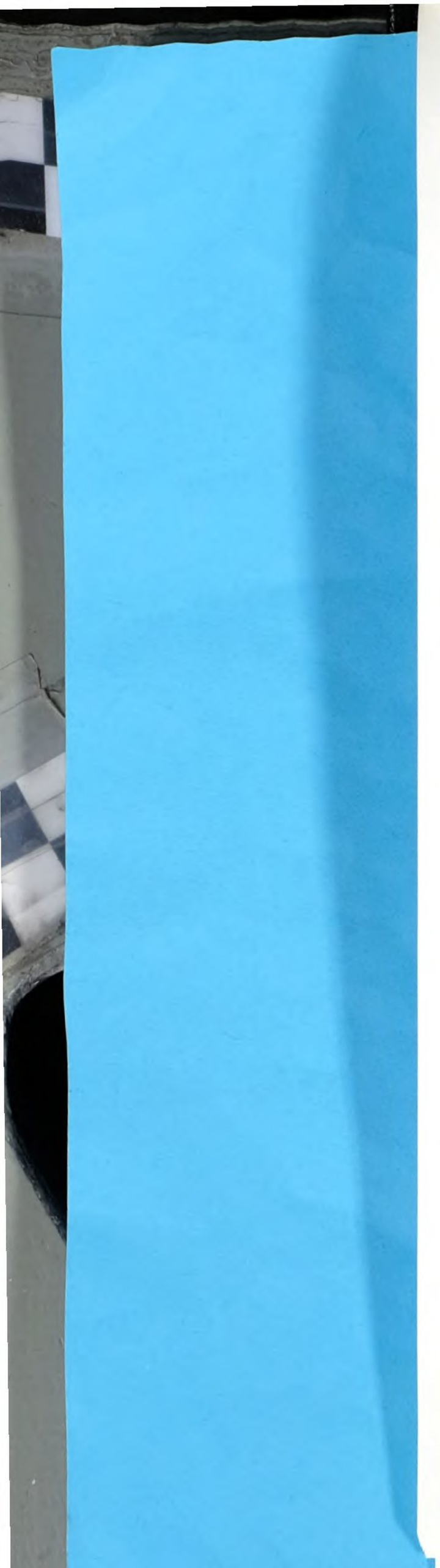

performed and no articles were found that coupled these two fiber applications to the study of engines. The only articles found dealt with the problems associated with inputting light from high powered lasers into a fiber optic, a technique known as coupling [5,6,7]. This problem is quite new as high power lasers and fiber optics have only recently encountered widespread usage. The difficulty occurs when high powered laser light is coupled or focused down into a single fiber because the intense energy from the laser burns the fiber. This problem will be discussed in greater detail in section 2.1.a.

Some recent work conducted on the use of high powered lasers and fibers has dealt with the coupling of neodymium: yttrium-aluminum-garnet (Nd-Yag) lasers into single fibers [5]. General Electric researchers, Marshall Jones and Gregory Georgalas, demonstrated that an intense beam of light from a Nd-Yag laser in excess of 400 Watts of average power could be coupled into a single fiber optic cable. G.E. has done this by devising a proprietary input coupler at the laser/fiber optic interface.

Medical applications with high powered lasers and fibers were conducted by K. Schonborn and W. Wodrich of SCHOTT Glasweke in Germany [6]. Researchers there developed a 'Universal' coupling device for all types of Nd-Yag lasers and different fibers. The coupling device is incorporated into the laser head and is adjusted during normal maintenance procedures. Thus, once the device is fixed, it does not need monitoring or adjustment to ensure good performance. With this device, SCHOTT obtained effective coupling with power transmissions of over 90% after coupling a 100W continous wave laser, and a pulsed laser, with a power density of 50 MW/cm^2. This means that only 10% of the light was lost between the input and the output ends of the fiber.

Finally, at the Institute of Electrone Technology in Warszawa Al Lotnikow, work has been conducted on the efficiency of coupling high powered lasers into fibers [7]. The single optical fibers tested ranged in various sizes and the efficiency of the coupling was found to be 12% to 44% (depending on the size of the fiber) and varied significantly

when the fiber was displaced with respect to the laser emission area. The study showed that as the fiber was moved away from the laser, less laser light was transmitted through the fiber. This implies that for good light transmission through the fiber, the fiber should be placed as close to the laser emission face as possible.

Most successful coupling devices are employed at or very near the emission face of the laser in order to control the environment between the laser and the fiber. By controlling the environment, burning hazards such as dust particles settling on the input face of the fiber can be avoided. The problems associated with the coupling of fiber optics will be addressed in the light input section (2.1.a) of this paper.

1.3 Fiber Optics

This thesis is presented as an introduction to the advantages and limitations of fiber optic applications in the study of internal combustion engines. Fiber optics are used as a method of transmitting information by reflecting light through optical fibers. They are used in place of access windows and conventional optics such as lenses and mirrors for a number of reasons. Some advantages over the more conventional systems include:

Elimination of the use of widows for optical access

Low light transmission losses

Reduced space and weight

Remote location measurement

Safety, by reduction of stray beams reflecting off mirrors

These benefits will be discussed in greater detail in chapter 2. For now, a simplistic description of a single fiber may help in the overall understanding of the benefits and

uses of fiber optics.

An optical fiber is a thin, flexible strand of transparent plastic or glass which carries visible light or invisible (near -infrared) radiation. This thesis will only focus on the discussion of light transmission through fiber optics in the visible region, though transmission is also done in the ultra-violet and the infrared regions. The infrared region is used for communication networking because of the low absortion losses in the fiber at that wavelength, and the ultra-violet wavelength is used for researchers studying phosphorescing materials.

An optical fiber consists of a central cylinder or core surrounded by a layer of material called the cladding, which in turn is covered by a buffer and protective coating. The core transmits the light wave, the cladding keeps the light in the core, and the cladding and buffer give the fiber it's bending strength and flexibility. (See figure 1.1)

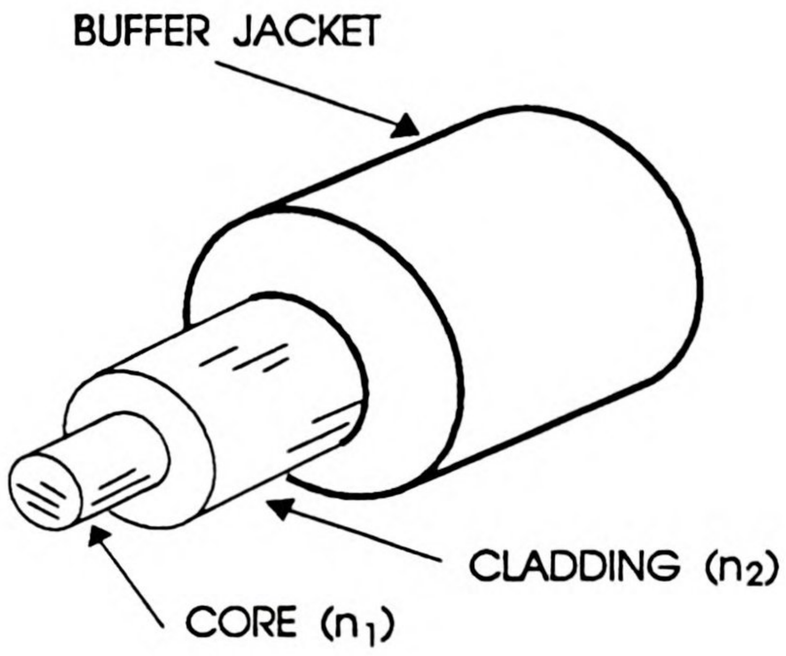

Figure 1.1 Schematic of a fiber optic.

The core, as well as the cladding is made up of either plastic, glass, silica or quartz. A fiber's core and cladding can be made up of any combination of these materials, the

most common being silica core and silica cladding. In comparison with glass, plastic fibers are flexible and inexpensive, can withstand greater stresses than glass fibers and weigh 40% less than their glass counterparts [8]. However, they do not transmit light as efficiently, and cannot withstand the energy associated with high power laser transmission. Therefore, glass fibers are used more frequently.

Optical fibers are quite small, comparable in size to a human hair. The core of a fiber ranges from 5 to 1000 μm, whereas the cladding diameters vary from 125 to 1800 μm. To keep the light within the core, the cladding must have a minimum thickness equal to the wavelength of the light transmitted [8]. The fiber core plays an important role in the design of an optical system and will be discussed in greater detail in section 2.1.b

An optical fiber works by allowing light to propagate along the length of the fiber by either reflection or refraction (the bending of light), depending on the type of fiber being used. Light propagates in free space at the speed of $c = 300{,}000$ km/s. In glass or other transparent materials, the speed of light is lower by a factor (n), known as the index of refraction of the material. The glass used for optical fibers has an index of about 1.5 Therefore the speed of light in the medium is

$$C_n = \frac{c}{n} \approx 200{,}000 \text{km/s} \qquad (1.1)$$

which is 33% slower than the speed of light through free space. When a light ray crosses the boundary between two materials with different refractive indicies, n_1 and n_2, the light is refracted or bent. This is expressed by Snell's law,

$$n_1 \sin\theta_2 = n_2 \sin\theta_R \qquad (1.2)$$

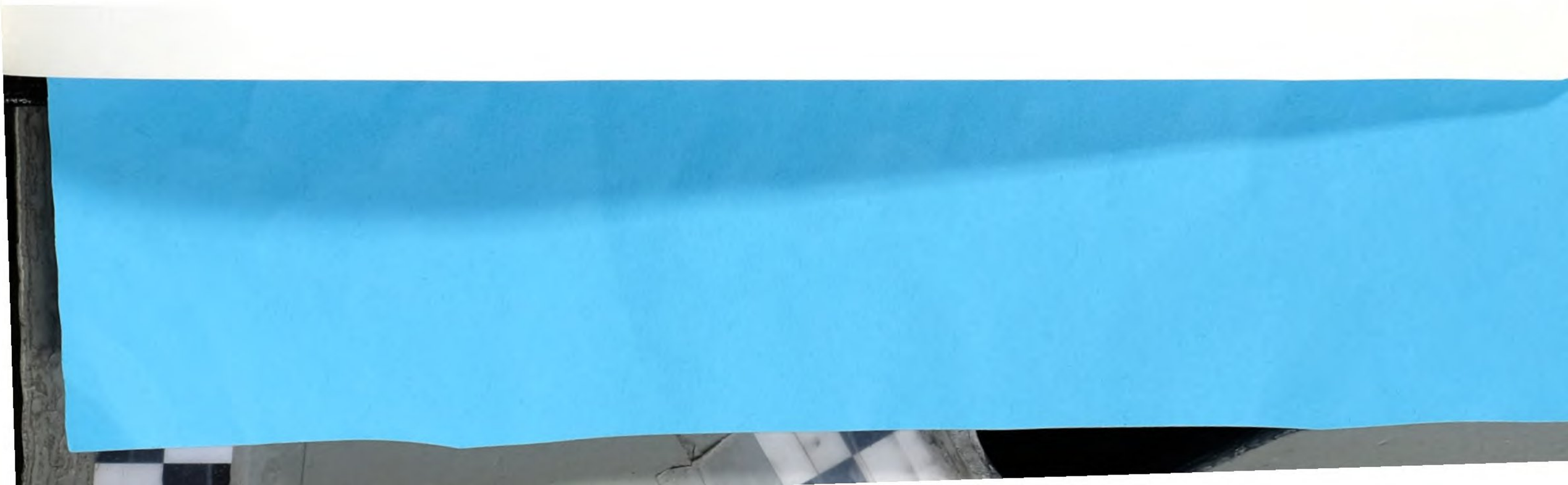

In optical fibers, the index of refraction of the core (n_1) is greater than the index of the cladding (n_2), causing the light ray to reflect back into the core when the light strikes the cladding/core interface at the correct angle. In figure 1.2 , rays 1 through 4 show different angles of incidence between the core and the cladding of the fiber. If light ray 2 crosses into the region of lower refractive index n_2, then the angle the light ray makes with the boundary (θ_R) becomes smaller than the original angle (θ_2). Eventually, if the original light ray angle (θ_4) becomes big enough, the refractive angle becomes zero and total internal reflection occurs (ray 4). Ray 1 transmits primarily through the interface into the cladding because it is perpendicular to the interface. The other rays start to reflect farther back into the core as the angle to the normal increases. At the critical angle, light is no longer refracted into the cladding but reflected into the core for total internal reflection.

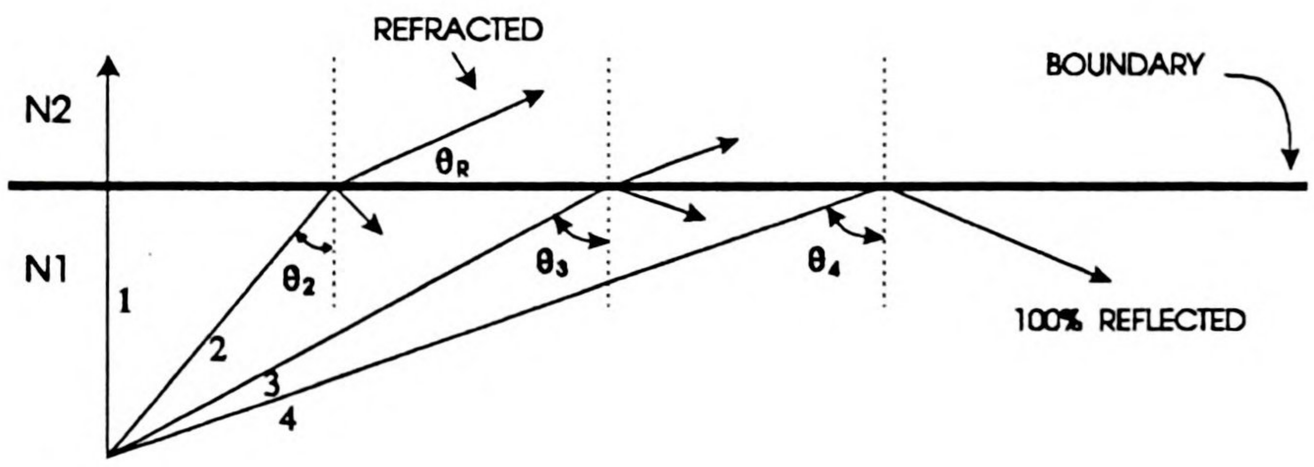

Figure 1.2 Reflected rays between the fiber core and cladding.

Fibers can also be described as step-index or graded-index fibers. These terms refer to a change in the index of refraction in the core of the fiber. In a step-index fiber, the index of refraction remains constant throughout the core. In the graded-index fiber, the refractive index changes throughout the core, and is highest in the center of the core decreasing radially toward the outer edge or cladding of the fiber. For step-index fibers,

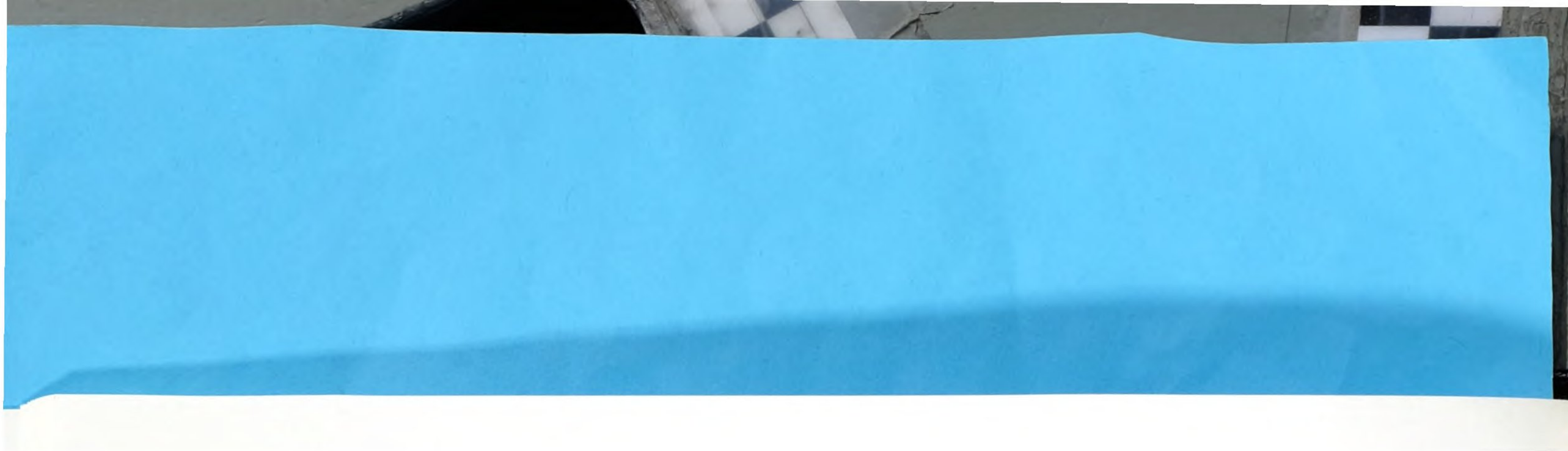

light traverses down the fiber in a zigzag manner through many successive total internal reflections. For the graded-index type, the light follows an undulating path because the direction of light is continually altered by virtue of the continuously varying refractive index [8]. In both cases, light is confined to the core. Figures 1.3a and b illustrate a ray trace diagram of light propagation through both a step and graded index fiber, respectively. Notice in figure 1.3a the abrupt change between the index of the core and the index of the cladding (in the index profile). This abrupt change is what gives the fiber the name "step-index".

There are also a number of paths or modes that the light can travel when propagating through the fiber. A single mode fiber means that there is only one path for the light to travel, and a multimode means there are several paths to follow. The size of the fiber core is what determines how many modes propagate through a fiber. Modes are actually solutions to the wave equation associated with the light entering the fiber. With a larger core, more components of the wave can branch out and propagate down the fiber. The angle at which each component branches off into the fiber, will determine the speed at which the mode traverses the fiber. Figure 1.3a shows a multimode step-index fiber with different mode propagation speeds.

For a graded-index fiber, the lag time between each mode is almost non-existent because of the continuously changing index of refraction in the core. As the light travels farther toward the outer edge of the cladding, the index value decreases, which allows the speed of the ray to increase. This change of refractive index allows for almost uniform propagation between modes, and gives the user a higher bandwidth.

For a light ray to propagate down the fiber, it must enter the fiber within a region called the acceptance cone. The acceptance cone is governed by the critical angle, which is the angle at which total internal reflection occurs in the fiber. From Snell's law, the

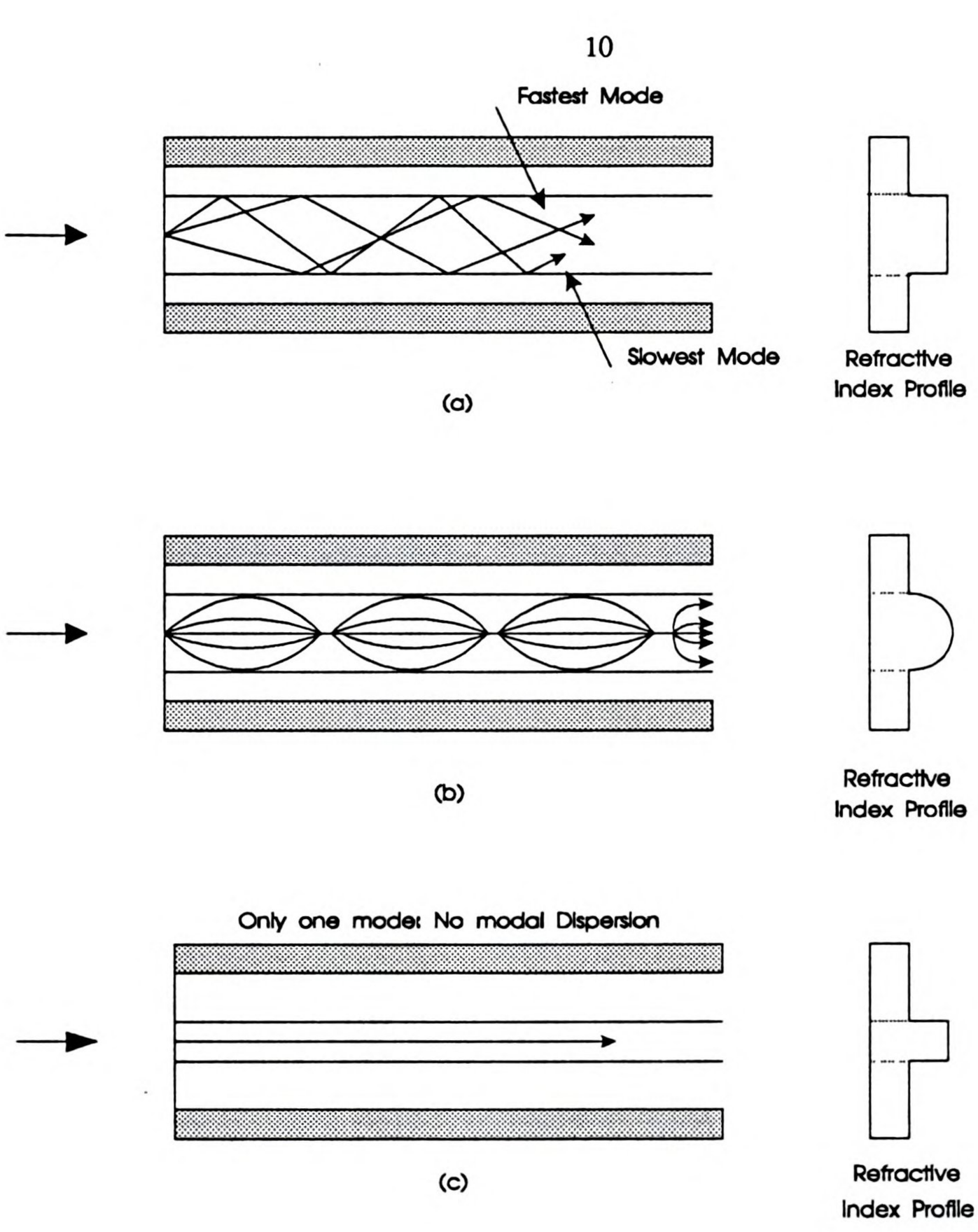

Figure 1.3 Different light propagation in fibers (a) multimode step-index fiber, (b) multimode graded-index fiber and (c) single mode step-index fiber. [8]

critical angle can be defined by,

$$\sin\theta_c = \frac{n_2}{n_1} \tag{1.3}$$

Figure 1.4 shows the propagation of light when it enters within or outside the acceptance cone. A light ray not within the acceptance cone will be lost in the cladding and never

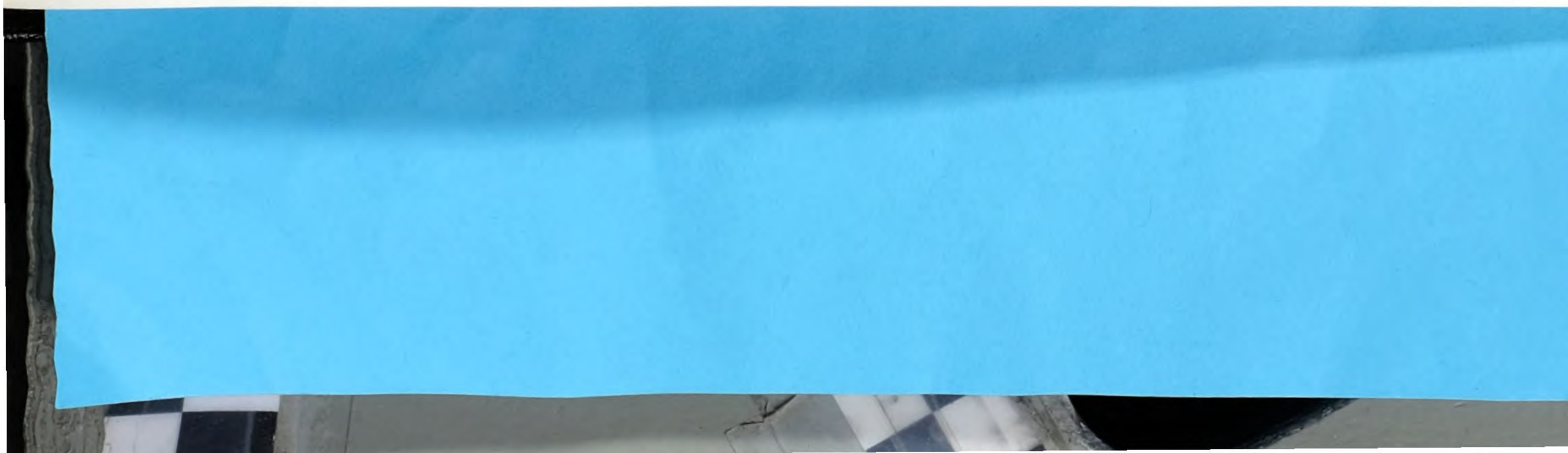

make its way down the fiber core. In the critical angle equation, n_1 is greater than n_2 and total internal reflection occurs for those rays at incident angles equal to or greater than the critical angle.

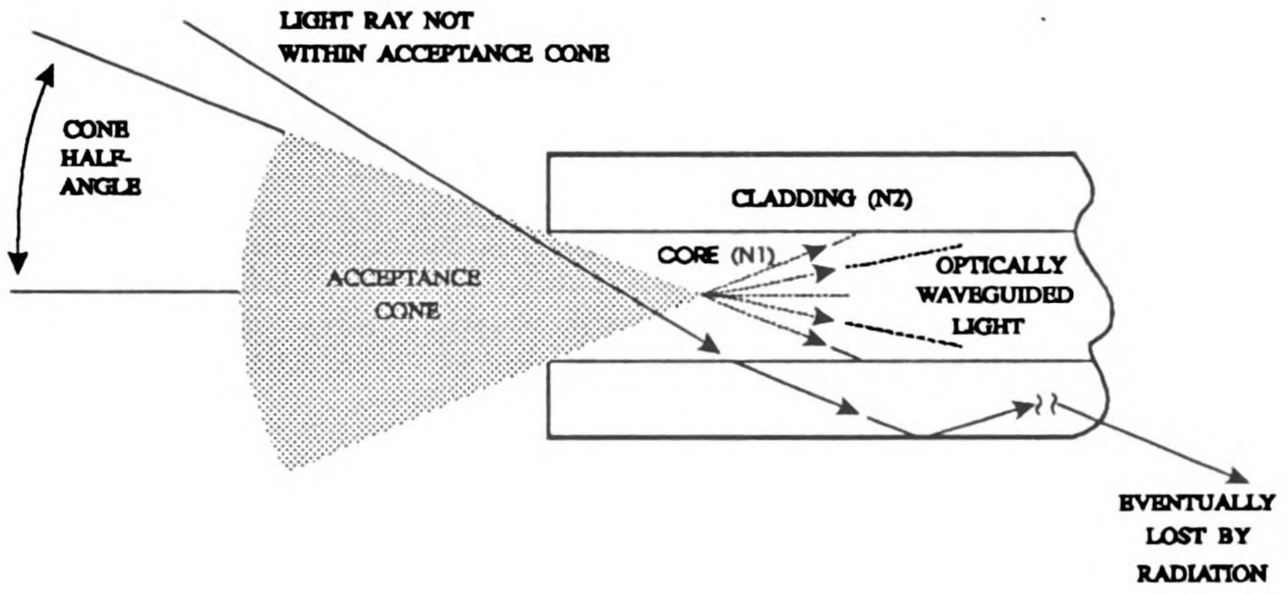

Figure 1.4 Optical fibers acceptance cone for incoming light [8].

Another way to describe a fiber is to refer to the fibers numerical aperture (NA). The NA is a measure of the light-gathering or collecting power of the optical fiber and is directly related to the acceptance cone angle. The larger the NA, the greater amount of light the fiber will collect. However, the disadvantage of a large NA is that as the NA increases, the bandwidth decreases. The NA is a function of the refractive indicies of the fiber, and it is always less than 1. For example:

For the step-index fiber,

$$NA = \sqrt{n_1^2 - n_2^2} \tag{1.4}$$

For the graded-index fiber,

$$NA = \sin\theta \tag{1.5}$$

Here, θ is the half angle of the acceptance cone of the fiber. The NA also indicates the efficiency of the source to fiber coupling. As the NA increases, the fractional amount of coupled light into the fiber also increases.

Transmission losses, or attenuation in optical fibers, are a very important parameter when considering the design of an optical system. The power of the light coupled into the fiber must fall off very slowly as it travels along the fiber. There are two principle causes for optical losses in glass fibers, (1) light scattering and (2) light absorption. Scattering losses arise from tiny spatial variations of optical density in the glass. A small fraction of the light traveling in the fiber is deflected from its path by these variations, and the light exits the fiber. [9].

Absorption arizes from various impurities in the glass. Compared to ordinary glass, optical fibers are remarkably free from imperfections, however, the impurities in a fiber absorb some of the light and convert it to heat. This absorption occurs only in the vacinity of certain wavelengths which correspond to the natural frequency of the impurity in the material. With upgraded manufacturing techniques these material impurities can be significantly reduced.

Losses in the fiber cause the optical power (P) to fall off exponentially with the length (L) of the fiber:

$$P(L) = P(0)\frac{-\alpha L}{10^{(10dB)}} \qquad (1.6)$$

Here P(0) is the optical power which couples into the fiber, P(L) is the output power of the fiber after length (L) and α is the attenuation coefficient which indicates the rate of loss of optical power. The product αL is often called the attenuation of the fiber. An attenuation of 3 dB means that by the end of the fiber the optical power out P(L) is only 50% of input power P(0) [9].

The optical losses previously described were a result of the properties and impurities of the glass. In addition, the geometry of the optical system can give rise to power losses. Losses are also incurred at the input and output faces of the fiber, where there is a 4% loss due to the reflection of the light as it passes through air (n_0) into glass (n_1). The greatest losses in optical fibers occur during the launching or input stage of transmission. The laser light must be aligned exactly on axis with the fiber and the light must be coupled into the acceptance cone of the fiber or it will not traverse down the fiber. All light loss in a fiber is known as attenuation and typically, attenuation is measured in decibles per kilometer (dB/km). Table 1 shows a comparison between the losses (attenuation) of three types of fibers.

To measure the attenuation losses in a fiber, a number of techniques have been used. However, most loss measurements do not indicate the method used to determine a fibers transmitting ability, and some methods may be very misleading. To accurately measure the losses associated with a fiber, the detector should be placed right at the input and exit of the fiber without any excess light influencing the detector. Measurements of light intensity in the units of W/cm^2 are the most useful because it is easy to calculate the power density on the face of the fiber when the laser beam size is reduced. When measuring intensity, the laser beam or fiber must be placed directly in the center of the detector. The detector must be flush and on axis with the fiber, or it will show a false reading. When care is taken to align the detector and the input light is coupled correctly into the fiber, all losses can be attributed to the fiber. However, if intensity losses are measured from light scattered off objects versus light directly coupled into the fiber, than other light loss factors begin to play a role, and the lack of light transmitted is not solely a result of the fiber.

The next section describes losses associated with image transmission through a collection of single fibers known as a fiber bundle. Coupling into a fiber bundle is critical to the success of flow visualization studies. The next section will also discuss

Table 1 Range of values for common optical fibers.

Type of Fiber	Numerical Aperture	Nominal Attenuation (dB/km)	Bandwidth (MHz-km)	Cost
Multimode, step- index	0.15 to 0.4	< 50	<25	Inexpensive
Multimode, graded- index	0.2 to 0.3	< 10	<200	Moderately Expensive
Singlemode, step-index	0.10	< 3 at 850nm < 1 at 1500nm	<2000	Expensive

light delivery through fiber optics and the problems associated with coupling high powered lasers into fibers.

CHAPTER 2

FIBER OPTIC APPLICATIONS TO FLUID QUANTIFICATION METHODS

The following sections discuss different applications involving the transmission of laser light through fiber optics into various test sites. The imaging of flow fields in these test sites using fiber optics will also be addressed.

2.1 Light Delivery Systems

Light delivery in fiber optics describes the transfer of light from a light source, such as a laser, through the length of a fiber to a test area. The input of light into a fiber, as well as the output from a fiber are complicated tasks and both need to be considered when designing a fiber optic system. When coupling light into a fiber, alignment between the laser and the fiber is critical. If a high powered laser is used, the intense energy from the laser beam will burn the fiber if alignment is not done properly. When light exits a fiber, it diverges into a cone shape. This light dispersal is not useful because current fluid flow analysis techniques generally require non-divergent light. The next few sections will discuss these problems in more detail and present solutions or alternatives for producing practical optical systems for fluid analysis.

A. Light input

The input or coupling of laser light into a fiber is perhaps the most difficult aspect of setting up a fiber optic system. Laser light can be coupled into a single fiber or a fiber bundle. In either case, the usefulness or quality of the light out of the fiber is dependant upon the precision coupling into the input face of the fiber. The following section

describes the desired geometric shape emitted at the output end of a fiber and which fiber system (a single fiber or a bundle) should be used to obtain this shape. This section will describe the technique of coupling laser light into a fiber and will also discuss the problems associated when coupling high powered laser light.

A single fiber is more difficult to couple than a fiber bundle because the size of the single fiber core or light receiving area is very small. The light beam from the laser must be focused to the exact size of the fiber core. The fiber must also be aligned on the same axis as the laser light in order to achieve coupling within the acceptance cone of the fiber. Remember from the earlier discussion that for total internal reflection along the path of a fiber, all light rays must enter the fiber within the acceptance cone. If the fiber is not on line with the laser, the light will not be focused to the correct position or spot size on the core of the fiber. Typically, focusing and alignment of the laser light to the fiber's input face is done with a microscope objective and an x-y-z translation stage. The microscope objective cannot have a numerical aperture greater than the acceptance angle of the fiber or all of the light will not enter within the acceptance cone. This is shown in figure 2.1, where the stray beam of light outside the cone gets lost in the cladding. Again, input

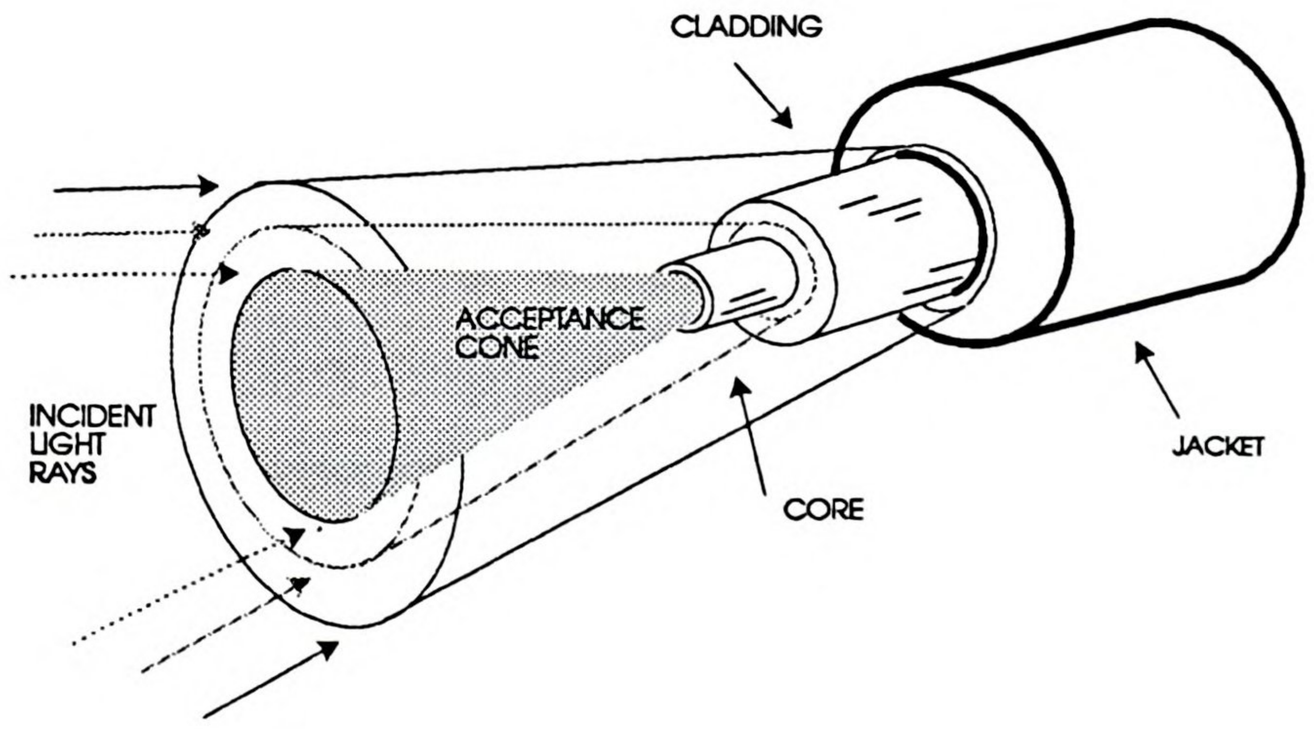

Figure 2.1 Light entering a fiber outside the acceptance cone.

light must be contained within this acceptance cone or the light transmission losses become excessive. The focal point of the laser light, which is directed through the objective lens is positioned just inside the fiber's input face. However, when laser light is focused down to a small spot size, which is slightly smaller than the core of the fiber, the power per unit area of the laser light increases greatly. This forces very intense energy into the fiber. If any of the focused laser light enters the fiber at the incorrect acceptance angle or gets trapped in the cladding or the jacket of the fiber, the jacket will burn and ruin the fiber. Nothing but the cladding and core of the fiber can withstand the high powered laser light. This high powered laser light causes other problems as well when considering burning effects. If dust particles settle on the input face of the fiber, then as the incoming light strikes the dust particles on the fiber face, the light is reflected off these particles at different angles outside the acceptance cone. This causes the high energy ray to be transferred into the cladding. Light rays that enter the cladding eventually travel further away from the core and into the outer jacket which burns from the high energy.

The same coupling problems that apply to single fibers apply to fiber bundles as well. As discussed previously, a fiber bundle contains a number of separate fibers arranged together in a single housing. Each fiber has a core and cladding and the individual fiber elements are held together by epoxy. A typical bundle arrangement is shown in figure 2.2.

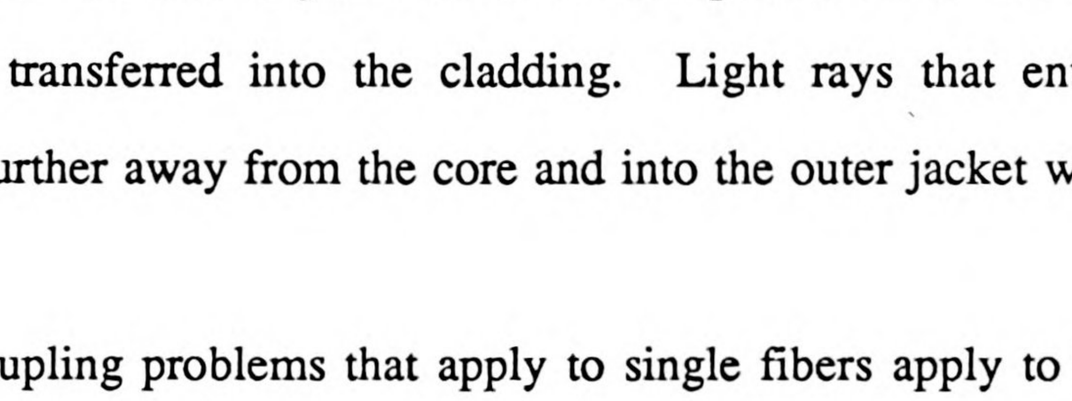

Figure 2.2 Input end of a typical fiber bundle.

When inputting light into a bundle, the image area or face of the fiber is quite a bit larger than a single fiber, therefore, light is much easier to couple into a bundle. A bundle utilizes an N.A. and acceptance cone similar to a single fiber, so again, the input light must enter within this cone. Typically, a microscope objective with an N.A. smaller than the bundle's N.A. is used to achieve the correct input angle. It is important not to misalign the axis of the laser with the bundle and not to expand the beam beyond the face of the fiber. This will cause light loss in the outer jacket of the bundle, just as it does in a single fiber shown in figure 2.1.

Problems associated with coupling high powered laser light into a bundle result from the interstitial, or locational spacing between the fibers. In figure 2.2, the spacing between each fiber consists of an epoxy filler which is used to secure the individual fibers together and insulate them from one another. This epoxy burns when high powered laser light is focused onto the input face of the bundle.

One method of overcoming the burning of the interstitial spacing inherent in the fiber bundle is to effectively reduce the area between the fibers. This topic will be discussed later in section 2.2 which describes a fused fiber bundle specially designed for high powered laser light.

B. Light output

When designing a fiber optic system, the desired light output from the fiber will determine what type of fiber to use and how many fibers will be needed. For internal flow studies in engine research, different light forms or geometrical shapes of light such as collimated beams or light sheets are needed for different types of analysis. An important feature to remember is that when these desired patterns of light are created with conventional optics, the collimated laser light coupled with lenses forms a clear, uniform light image. When an optical fiber is used to deliver the laser light, the quality

or uniform intensity of the final light form is significantly reduced. In fact, the intensity of the light output from the fiber is analogous to a bad flashlight. The light out of a multimode fiber tends to appear as if it is flickering, with spots of dim or bright intensity in the beam. This is a result of the multimode fibers used to transmit the light. Different modes transmit the light at different speeds, causing non-uniform intensity to appear at the output face of the fiber. Lack of uniform intensity is an inherent property associated with multimode fiber optics and must be considered when designing a system that requires light uniformity. Because of this problem, the properties of the final light output from a fiber may not be suitable for certain systems. Therefore, it is important to investigate flow quantification methods using laser light to see if fiber optics can enhance the existing light delivery techniques. The following sections will discuss different types of fluid flow analysis methods, their requirements for light output, and what types of fibers may be useful as replacements for conventional optics.

(1). Introduction to Flow Visualization Using Fiber Optics

There are many types of flow visualization techniques, such as holography, interferometry and the Schlieren method. At the MSUERL, flow visualization involves observing light scattering from particles which are assumed to follow the flow. This qualitative analysis method is accomplished by filming the fluid motion. For internal combustion engine work, high frame rates are desirable in order to visualize the real time movement of the fluid particles. For this technique, a thin sheet of laser light is directed into the engine or test area, and the fluid flow inside the engine is illuminated by seeding it with either smoke particles or microballoons - both of which reflect light. This sheet of light illuminates the seeded particles in a plane and a high speed camera films the motion of the particles as the light scatters off them. The light sheet is created by directing the laser light through a series of lenses and mirrors. In order for the light to

enter into the engine and the motion of the particles to be filmed, two windows must be inserted to replace portions of the engine housing. One narrow window allows the light sheet into the engine, the other window is located perpendicular to the light sheet so that viewing of the flow field illuminated by the sheet can occur (see figure 2.3). The filming of the particle motion is done with a high speed camera which can capture events at frame rates of 5000 frames per second and higher. This high speed camera is needed to record real-time measurements of the fluid motion. The optical system must be configured to provide sufficient light to expose the film. This will depend on the light source, losses in lenses and mirrors, the particle scattering efficiency, the viewing angle and the camera's light collecting ability. Using conventional photographic film, this high energy can only be obtained by using a high powered directed light source such as a copper vapor laser.

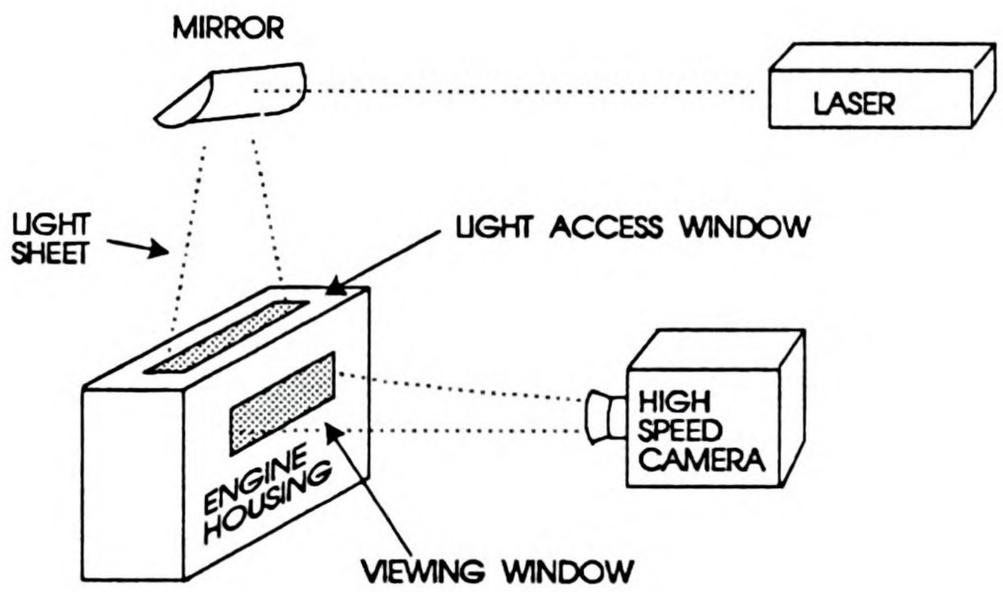

Figure 2.3 Light delivery and imaging in a flow visualization system.

The next few paragraphs describe some advantages to using a fiber optic system over conventional optics for light delivery in a flow visualization system. For planar flow visualization in engines, fiber optics can reduce the need for a large window which is used with conventional optics to get the sheet of laser light into the engine. The drawbacks of these windows are outlined in section 1.1. The output end of the fiber

could actually be placed in the engine. Then a series of small lenses placed in a coupling device just after the output face of the fiber would be used to transform the diverging cone of light out of the fiber into a thin sheet of light. By replacing the large window with a small fiber, leakages associated with misalignment between the window and the engine housing boundary would be significantly reduced. With a fiber, the fiber/housing interface boundary would be much smaller, thus producing less interference with the flow field and ultimately a more accurate representation of the fluid motion.

Other benefits that optical fibers could bring to the flow visualization technique are remote location measurement and ease of optical setup. Fibers are very flexible and can be wound through almost any test configuration, making light delivery to hard to reach areas quite simple. With the use of fibers, the number of lenses and mirrors are reduced and lens aberrations, light losses, time required for setup, and optical alignment would be significantly reduced.

The aforementioned benefits detail how fibers could be an ideal replacement for the conventional optics used in flow visualization. However, actually creating a sheet of light from a fiber requires that the light out of the fiber be coupled into two lenses separated by a critical distance. This introduces many problems because the critical distance depends on the lenses used, and the desired width and thickness of the sheet. For a typical configuration used at the MSUERL, the fiber would have to be removed from the engine and set back away from the housing by about 2 or 3 cm in order to achieve the desired light sheet width of about 10 cm. This removal of the fiber is due to the focal length of the collimating lens which requires a lens separation of at least 2 cm to obtain the 10 cm sheet of light in the engine (see figure 2.4). Once the sheet is created, then a window would be needed to input the sheet into the engine. Figure 2.4 shows that the lens system needed for the fiber system is as complicated as the conventional optic system, which needs a cylindrical lens to create the sheet of light and a cylindrical mirror to spread the sheet. The focal lengths in figure 2.4 play an

important role. This optical arrangement involves lenses with very short focal lengths (excluding micro-lenses which cannot create a wide enough sheet of light). The sheet of light spreads quickly with a small focal length cylindrical rod. Figure 2.4 shows that as the focal length of the cylindrical rod increases (from 5mm to 10mm), the light sheet spreads much slower, achieving around a 5 cm spread as it nears the engine. The slower the sheet spreads, the farther the fiber optic and lenses must be placed from the engine. This tends to defeat the purpose of using fibers because the optical access window is not reduced. Therefore, when considering the final fiber optic system, the only benefit over conventional optics is that the fiber system can be used for remote location measurement.

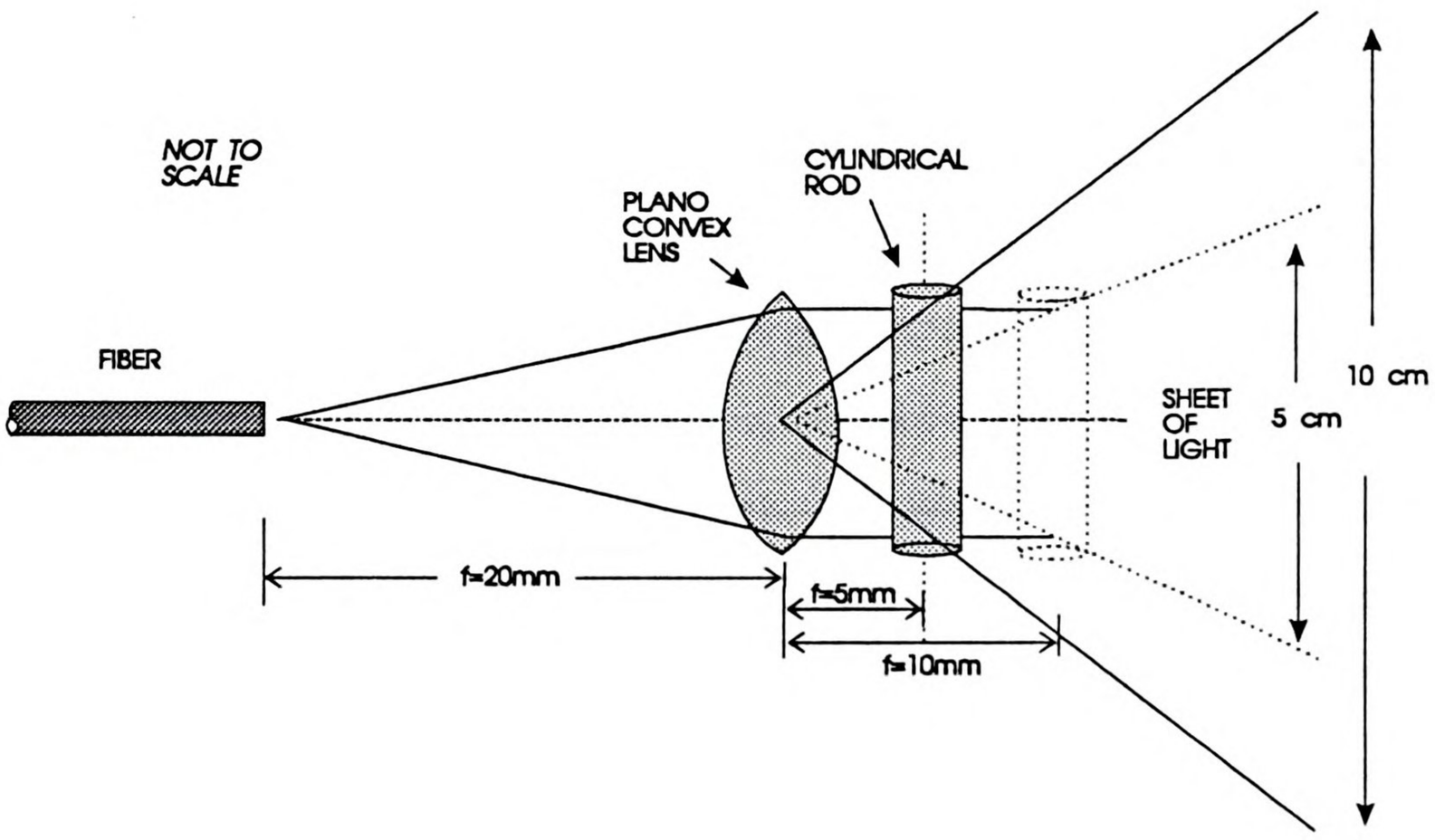

Figure 2.4 Fiber optics in flow visualization

(2). Particle Image Velocimetry (PIV)

Although the flow visualization technique offers substantial insight to the behavior of the flow field, it is more desirable to conduct a study that allows one to obtain

quantitative velocity data at many points simultaneously. Particle Image Velocimetry (PIV) provides the ability to measure two dimensional velocities over an extended planar region [9].

In a typical setup, PIV requires the use of a sheet of light about 15mm in width and 300 μm in thickness. As particles pass through the light sheet an image of the particles within the light sheet is photographed with a 35mm camera. The type of laser used is normally an Nd-Yag laser which has high energy per pulse and good light quality or intensity distribution throughout the beam. The laser beam is double pulsed with a pulse separation of about 30 ns and a pulse duration of about 20 ns. The double pulse creates a photographic negative containing two images of each particle. By interrogating small sections of the light sheet within the photograph, the distance and the direction that the particle travels can be tracked and measured. The average velocity vector of the particle can then be calculated by knowing the distance it traveled and the time it took to travel that distance (time separation between laser pulses).

For this technique, as in flow visualization, a sheet of light is needed to illuminate the motion of the fluid particles. However, the sheet of light required for PIV is quite small in size and very thin, about 300 μm. This is about the thinnest sheet of light that can be obtained by conventional optics. The same optical system that was designed for flow visualization is also needed for PIV (see figure 2.3), but the focal lengths and lens separation distances would be smaller to achieve the smaller light sheet. The critical problems arise in creating the thickness of the light sheet. PIV requires the sheet of light to be around 300 μm thick which is impossible to obtain using a fiber optic system. A fiber system can only obtain a sheet of about 2 mm thick. Therefore, this light delivery analysis technique is not possible using fiber optics as the delivery system.

(3). Laser Induced Photochemical Anemometry (LIPA)

Another fluid analysis technique which acquires velocity data at many points simultaneously is LIPA (Laser Induced Photochemical Anemometry). LIPA is used to measure velocities and velocity gradients over a chosen plane of fluid motion. The technique consists of tracking a fluorescing grid created by laser lines directed into the flow. These laser lines are generated initially by splitting the collimated laser light into two separate collimated beams using a beam splitter. These beams are then directed onto two stepper mirrors which divide the incident light beams into an intersecting grid pattern . Each beam in the grid pattern has a diameter of about 0.5 mm [1]. The optical setup is shown in figure 2.5a.

The main optical problem with this technique is that a window must be inserted into the engine housing to allow the light to enter. Also, the stepper mirrors used to direct the light into the engine housing exhibit reflective light loss and are difficult to create and align. As discussed previously, viewing windows inserted into an engine housing are difficult to align and expensive to put in. If a fiber bundle were used, it would eliminate the need for a window in the housing of the engine. The output end of the fibers would be placed in the housing and the face of the fibers would be flush with the inner chamber of the engine. These small inserts for each fiber would cause very little disruption of the flow compared to the large widow used with the stepper mirrors. A bundle would also reduce the amount of mirrors, lenses and alignment problems associated with stepper mirrors because once the light is coupled into the bundle, the alignment work is done. Figures 2.5a,b compare the different optical arrangements for the stepper mirror LIPA technique and the fiber optic technique.

In a performance comparison with stepper mirrors, fibers alleviate reflective light loss that is associated with stepper mirrors as the light travels from the output of the laser to the input of the engine. However, in the study conducted with stepper mirrors, no

final intensity measurements were taken so a complete comparison of light transmission losses cannot be evaluated. Also, fiber optics cannot reduce the individual beams size smaller than about 2 mm. The LIPA technique using stepper mirrors, again, can reduce the beams to a diameter of 0.5 mm.

The feasibility of the LIPA technique using fiber optics depends on a number of different things. Both the output and the input ends of the fiber bundle must be carefully considered due to the complexities of coupling high powered laser light and the desired light output needed to capture the particle motion for this fluid analysis technique. These problems will be discussed in further detail in the fused fiber bundle section (2.2) of this paper.

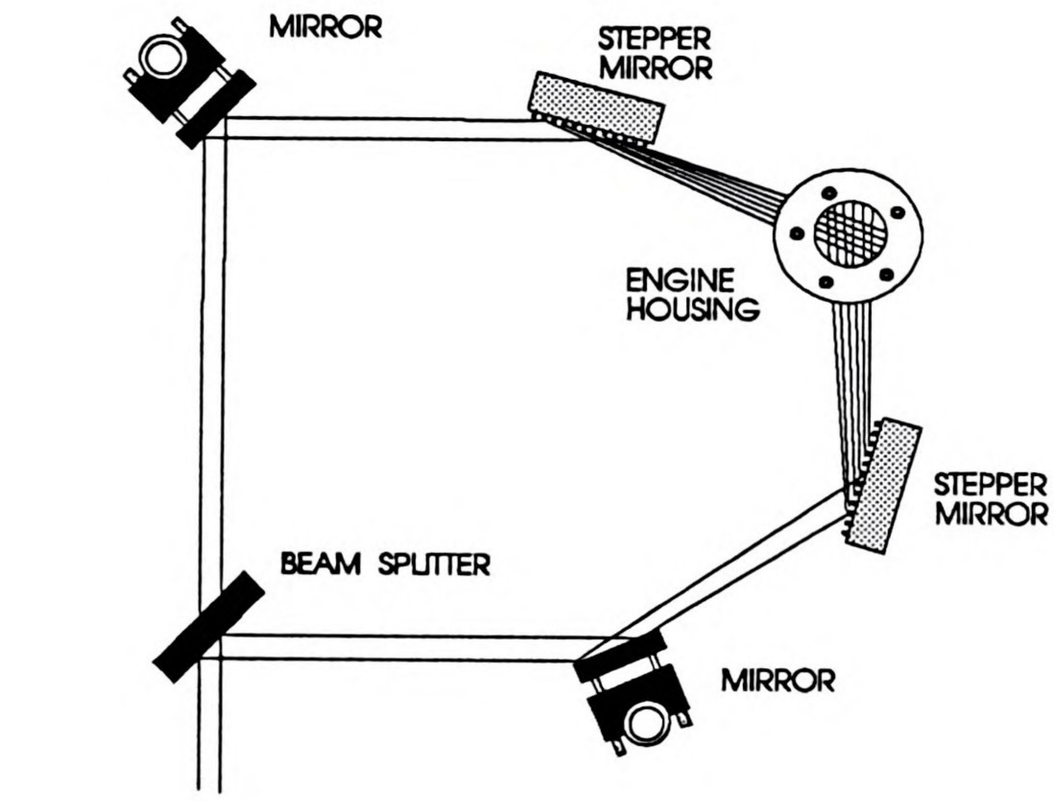

(a)

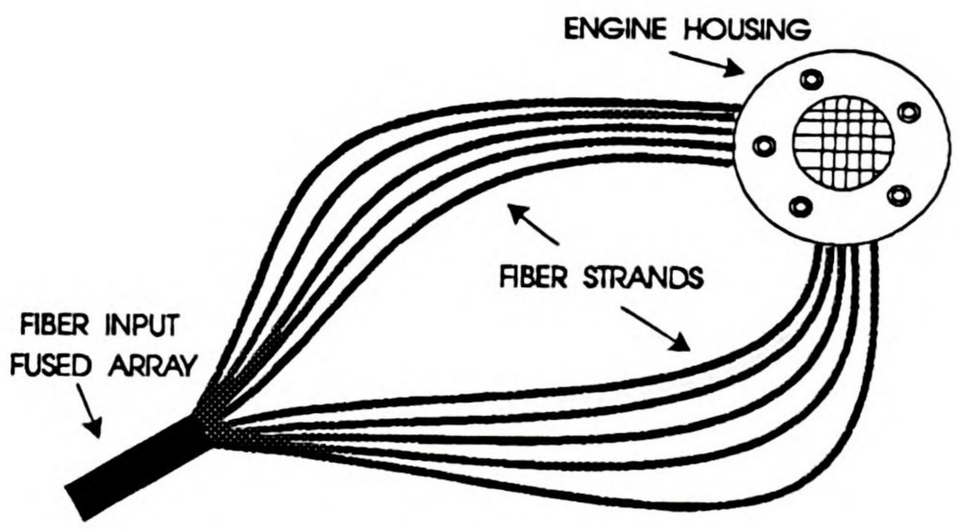

(b)

Figure 2.5 Optical arrangement for the LIPA technique using a) stepper mirrors and b) fiber optics.

2.2 The Fused Fiber Bundle and its Application To LIPA

From the previous discussion on light delivery, the desired output of the optical system will determine what type of fiber optic system to use. For both flow visualization and PIV, the benefits obtained by using a fiber system are minimal because the lens combination requires the fiber to be removed from the engine. However, a fiber optic design appears to be ideal for LIPA since the grid pattern of light needed for the LIPA technique does not require the fibers to be placed away from the engine housing. A brief description of the light requirements for the LIPA technique regarding input and output will follow as well as assembly procedures of the chosen system and a discussion of its performance.

A. Description of a fiber bundle

The design of the input face of the fiber bundle is critical because of the possibility of burning the interstitial spacing between fibers. A typical fiber bundle designed for high powered laser applications is shown in figure 2.6. This particular bundle was custom designed by C-Technologies Corporation for the unique purpose of coupling high powered laser light. The bundle is made from seven individual fibers fused at the input end and free at the output end. These individual fibers are silica core, silica clad, step-index, multimode fibers with a core diameter of 100 μm and a cladding diameter of 125 μm. What makes this bundle unique is that the input end or fused end of the fibers have their jackets stripped back about one inch from the front face of the bundle. This leaves only the core and cladding exposed to the high energy input light. In order to fill the gaps between the fibers caused by stripping back the jackets, the fibers are heated and molded together. This technique is known as fusing. The silica core of each fiber tends to melt and deform. As the fibers deform, they mold together in a tight fit. A picture of

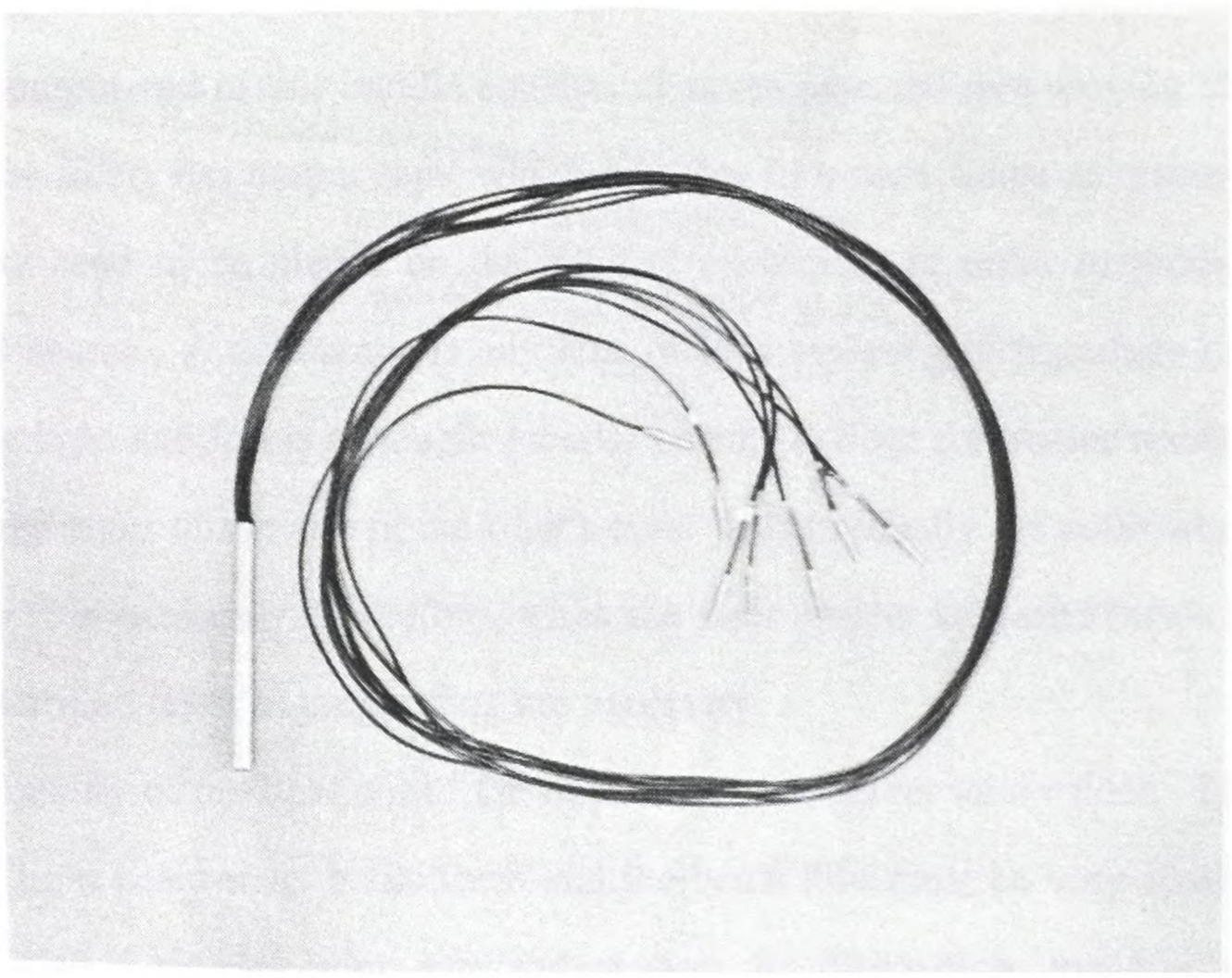

Figure 2.6 Fused fiber bundle for high power laser coupling.

the front face of the fused fiber bundle is shown in figure 2.7. Notice the deformation of the once circular fibers. The stripped portion of the input configuration of this bundle allows the high energy light to enter the seven slightly deformed fibers and reflect internally without burning the jacket and epoxy. However, there are disadvantages associated with the fusing technique and they will be addressed later in this section.

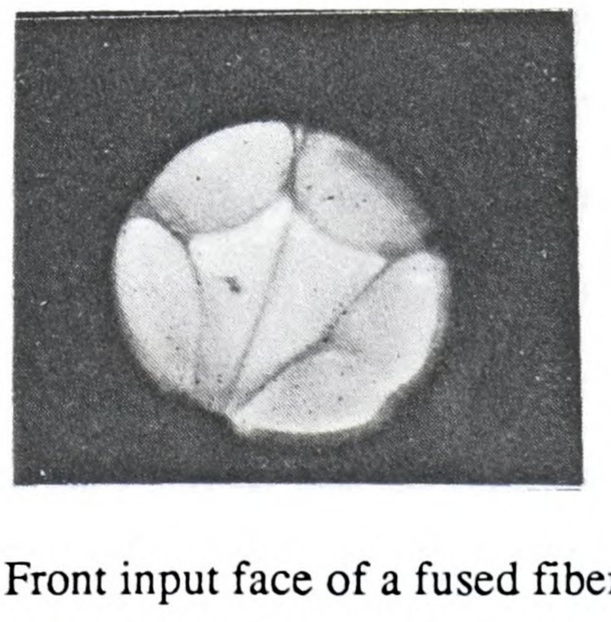

Figure 2.7 Front input face of a fused fiber bundle.

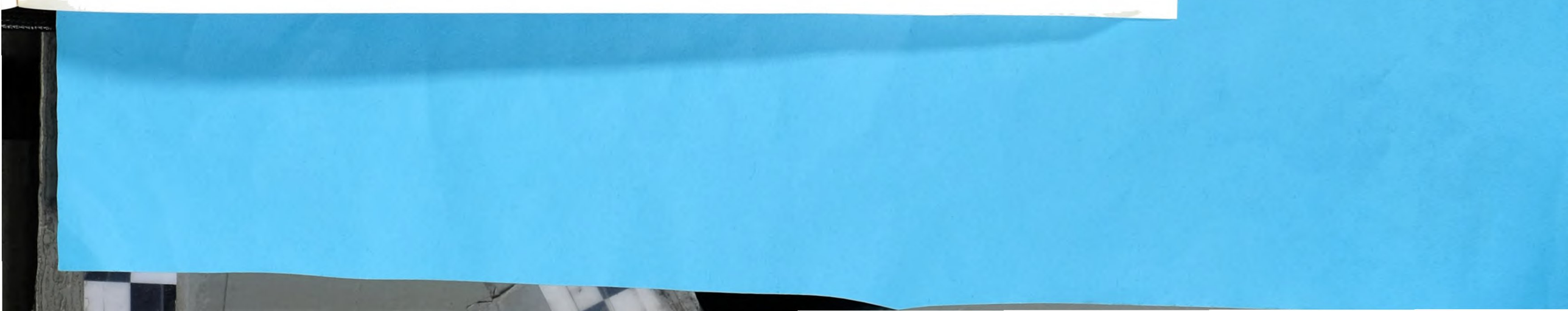

The output end of this bundle consists of seven jacketed free moving fibers. Each one of these fibers has output light which diverges in a cone shape as discussed earlier. Collimators need to be placed on the ends of each fiber in order to produce parallel collimated beams. A collimator is any lens or lens system which gathers diverging or converging light and forms a straight parallel beam. A fiber collimator needs to be very small; on the order of the size of the fiber's outer jacket. Ideally the collimator should fit the fiber core size exactly. Therefore, when the fiber system is placed inside the engine, only small drilled holes in the housing are necessary.

The quality of the light out of the fiber is another matter to consider. The intensity from each light beam must be uniform and the beam size must be very small, around 1 mm. Creating a smaller beam size and placing the fibers close together results in a smaller grid pattern, which allows for a more detailed analysis of the flow when using the LIPA technique. With LIPA, each grid box represents an average velocity for the given area inside the box. If a smaller area is analyzed, a more accurate picture will result. Ideally, the grid size is analogous to the fluid particle itself.

In order to fill the small size requirement for the LIPA technique, the collimators that were chosen to fit on the ends of the fiber bundle were a graded-index (GRIN) lens manufactured by NSG Corporation. The theory behind these lenses is that the index of refraction of the lens continuously changes, just as it does in a graded index fiber. This gives the light a continuous bend during refraction and depending on the change in the index, the desired output (collimated light) can be achieved within the length of a single rod-shaped GRIN lens versus a multiple lens system. Figure 2.8 shows a GRIN Lens continuously changing its index of refraction.

It should be mentioned that the LIPA technique requires the use of ultra-violet light (wavelength of 350 nm) to excite the phosphorescing particles in the flow field. However, GRIN lenses only work at wavelengths greater than 380 nm. The manufacturers did comment that unofficially the GRIN lens could work at 350 nm. With

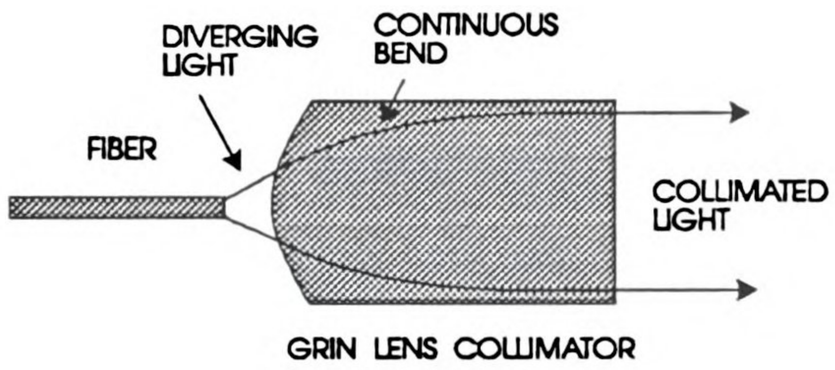

Figure 2.8 GRIN lens with continuously changing index of refraction.

this in mind and discovering that GRIN lenses are the fibers industries universally accepted collimating technique, the lenses were purchased for the LIPA technique. It was important to discover how effective these lenses were at collimating light out of a fiber.

These lenses can be purchased from NSG Corporation already assembled onto a fiber optic cable, or the collimators can be purchased separately and assembled later onto any desired optical fiber. For this study, the fused fiber bundle was manufactured by C-Technologies, so the pre-assembled fiber system with the collimating GRIN lenses could not be used. Therefore, M-type collimators, or user assembled collimators were purchased to fit over the output ends of the bundled fibers. A schematic of the GRIN Lens collimators is shown in figure 2.9.

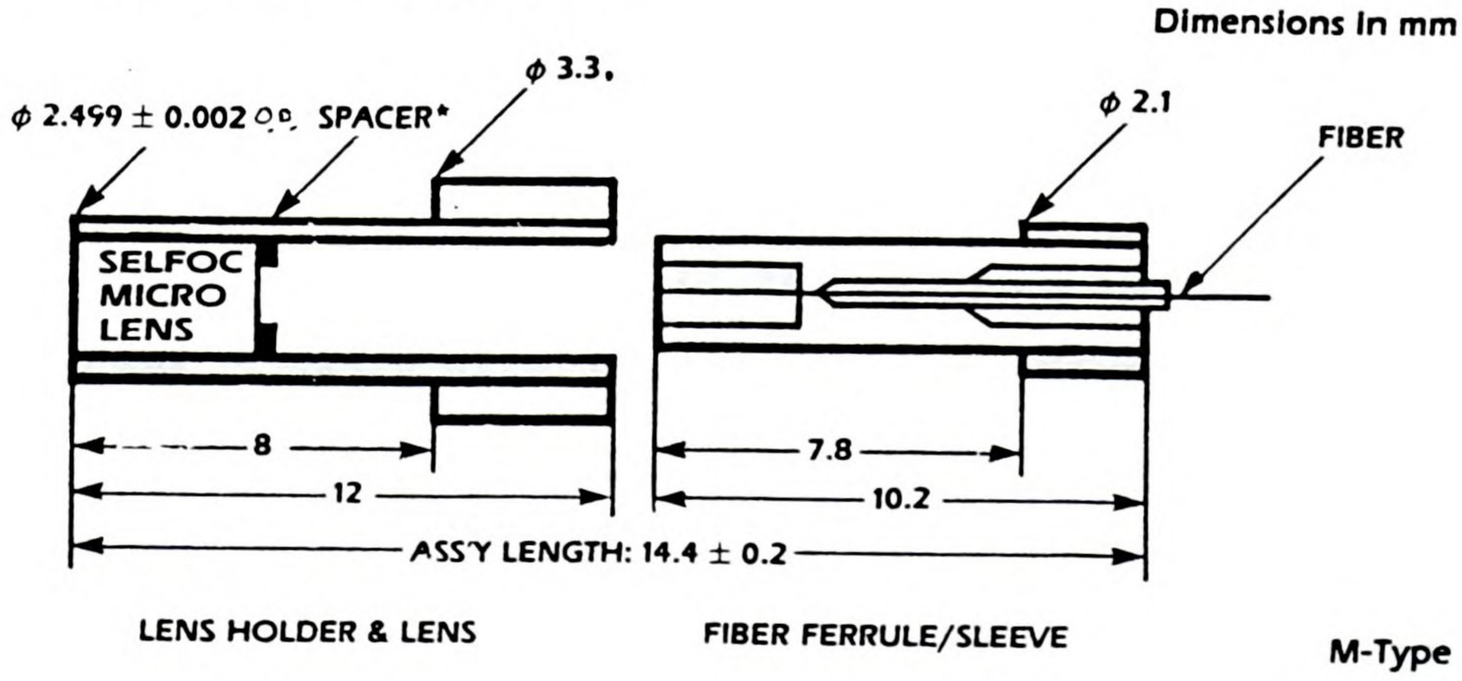

Figure 2.9 Schematic of an M-type collimator.

The core size of the fibers played an important role in determining the feasibility of utilizing the technology of a fused input bundle with collimating lenses. During the fusing procedure, heat and the pressure applied to the fibers was done in moderation in order to prevent the fibers from melting too much or cracking. C-Technologies will not fuse fiber cores smaller than 100 μm because a smaller core fiber can not withstand the pressures that occur during the fusing process. Ideally, they would like to fuse core sizes of 400 μm or greater. On the other hand, the GRIN lens collimators work best with a small core fibers because the small fiber cores act much like a point source. It is much easier to collimate a point source than it is to collimate a diverging beam. Because of this, NSG does not manufacture M-type collimators for fibers greater than 100 μm. Therefore, the fiber bundle used in this study was comprised of 100μm core fibers.

The M-type collimators purchased for the bundle must be assembled by the user. However, the assembly procedures require tools for cutting and polishing the fiber ends. Since the tools were not available at Michigan State University, the bundle was taken to NASA Lewis Research Center and the collimators were mounted to the output end of the seven fibers with the aide of their technicians. The next section will discuss the assembly procedures for attaching the collimating lenses and the last section will talk about the overall performance of this unique bundle.

B. Assembly of GRIN lens collimators

The core and the cladding size of the fiber must fit the collimators pre-manufactured size. A core of 50 μm and a cladding of 125 μm was available, as well as a core of 100 μm and a cladding of 140 μm. The fibers in the bundle have a core of 100 μm and a cladding of 125 μm. It is important to match the cladding size of the fibers with the collimating lens because this is what determines the proper position of the fiber in the collimator assembly. The core size is not as important because the GRIN lens is

much larger than either the 50 μm or the 100 μm core fiber. This larger size allows the GRIN Lens to capture and collimate all of the light out of the fiber, no matter what size is used. Therefore, the core to cladding ratio of 50/125 μm was chosen to match the fit onto the bundle.

In order to assemble the collimators onto the fibers, the fiber was cut and the jacket of the fibers was stripped back to fit into the metal sleeve or ferrule of the collimator assembly (see figure 3.4). The fiber also must be centered in the ferrule to achieve proper alignment with the GRIN Lens. The ferrule slides over the fiber and epoxy is placed around the fiber to hold the ferrule in place. The ferrules diameter should be 128 μm (although after the system was assembled and measured, it appeared to be 140 μm). Figure 2.10 (a) and (b) show the front and side view of the fiber in the ferrule. From the front view in figure 2.10 (b), it is quite evident that the fiber was not centered properly in the oversized ferrule.

Once the ferrule is securely in place, the fiber must be polished. To polish a fiber, usually three different grades of sandpaper are used until virtually no scratches are left on the face of the fiber. Polishing must be done carefully to prevent the metal ferrule shavings from dragging across the face of the fiber and scratching it. If the fiber is scratched, the ferrule must be cut off and the assembly procedure started over again with a new GRIN Lens collimator.

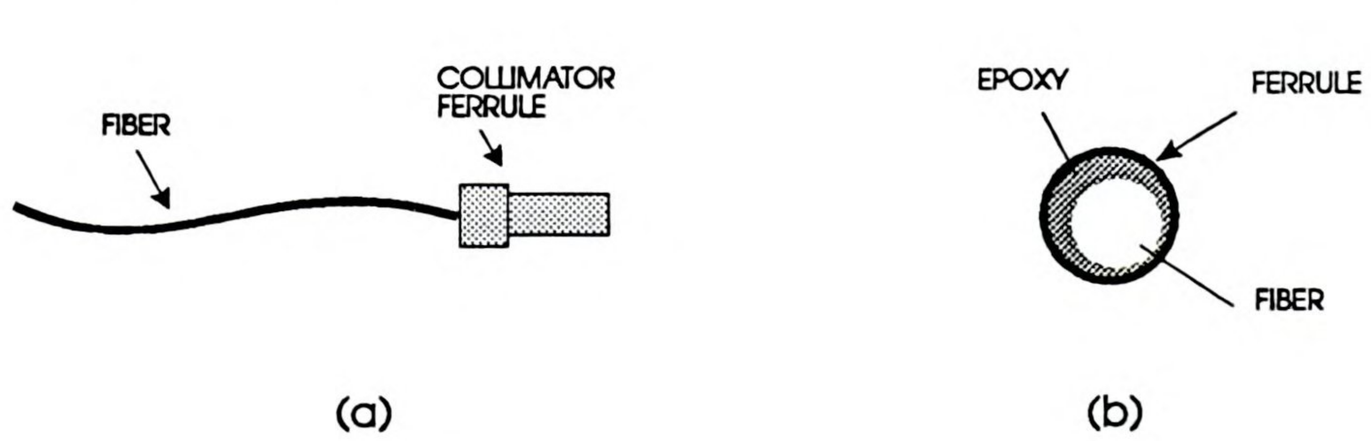

Figure 2.10 GRIN lens assembly with a) the fiber in the ferrule b) the front face of the fiber showing the off-center alignment of the fiber in the ferrule.

After the fiber is polished, a spacer is inserted into the collimator holder which contains the GRIN lens (refer to figure 2.9). This spacer separates the polished face of the fiber from the GRIN lens by 40 μm, a distance which is critical to the collimating efficiency of the GRIN lens. The fiber then slides into the holder and rests up against the spacer. Epoxy is used to secure the fiber in place.

This assembly procedure is quite tedious because each fiber must be assembled separately and great care must be taken when working with such small diameters and distances in order to achieve the best performance. The next section will discuss the performance of these collimators as well as the performance of the fusing technique.

C. Performance of the bundle

The main reason for the design and application of the fiber bundle to the LIPA technique is to collect high powered laser light and emit several parallel collimated beams to form a grid pattern of light. To check the collimating ability of the GRIN lenses, a low power Argon laser was coupled into the fiber bundle. The light that emerged from each of the fiber ends diverged at a rate of about 2.8 degrees. This small divergence angle doesn't seem like much, but a very small core size (approximately 100 μm), with a divergence angle of 2.8 degrees over a light transmission length of 6 inches results in a beam size about 10 times larger than that at the output face of the fiber. For the LIPA technique, because the grid pattern needs to be very small and extend over a distance of about 2 to 8 inches for engine studies, this divergence is unsatisfactory.

A number of reasons may contribute to the disappointing results of the collimating attempt. NSG expects some divergence with every collimating system, and the larger the core size of the fiber, the more divergence there will be. NSG predicts a divergence of approximately 2 degrees for a 50/125 μm fiber system [10]. A larger core size of 100 μm, will contribute to an even higher divergence angle. There are a number of other

factors that will also increase the divergence rate. Examination of the schematic in figure 2.10 (b) illustrates that the fiber is not centered in the collimator's ferrule. In this example the ferrule being used is oversized (144 μm instead of 128 μm). This creates a misalignment or loose fit which causes the light exiting the fiber to be off center when entering the GRIN lens. The GRIN lens will not perform as well under these conditions. If the core size of the fiber is not directly on line with the spacer, the light exiting from the fiber may be partially blocked by the spacer.

There are a few other problems that may contribute to the divergence of the light. The divergence equation given by NSG is dependent on wavelength [10]. The GRIN lenses purchased came with a standard coating for a wavelength of 633 nm which matches the wavelength for Helium-Neon (HeNe) laser light. If the lens was coated with a 514 nm (Argon laser light) wavelength, greater divergence would occur with the non-matching Argon wavelength. A test was conducted to compare the divergence rates of the HeNe laser versus the Argon laser. The test showed that the HeNe wavelength collimated 1 degree better than the Argon laser. This confirmed that the GRIN Lens was coated to match the wavelength for HeNe.

Because of the disappointing performance of the output of the fiber bundle, this light delivery system could not be used for the LIPA technique. Even though the light out of the fiber can be collimated using external lenses placed beyond the GRIN lens, the beam diameters are still too large to be used for LIPA. The only other alternative solution to the diverging problem would be to try to add micro-lenses (very small lenses with short focal lengths) to the output end of each fiber to collimate the light emitting from the fiber.

Since the output light from the fibers in the fused bundle could not be collimated, there seemed no reason to risk the destruction of the bundle by coupling the high powered laser light into it. The reasoning behind this was that if the bundle were tested and destroyed, it would be very difficult to determine what actually caused the failure.

First of all, failure could occur if the light weren't focused to the correct spot size on the bundle, allowing the overfill light (outside the core) to burn the outer epoxy and jacket. There has also been some concern that the light in each fiber will jump the cladding of the other fibers. This was illustrated by coupling laser light into the output end of a single fiber from the fused bundle. All seven fibers on the fused input end were illuminated by the single fiber as shown in figure 2.11. This means that throughout the

Figure 2.11 The entire input face of the bundle illuminated from light entering one fiber at the output end of the bundle.

one inch fused section, light was transmitted from fiber to fiber (i.e. light jumped the cladding). The concern is that after the light is transmitted past the fused region, the power may still be too high for the epoxy. The epoxy is located in between the individual fibers after the fused region and if the high energy light eventually jumps into the epoxy, the bundle will burn. These are the numerous problems that may cause the bundle to burn, but without the proper examining tools, it would be impossible to discover which factor caused the ultimate failure.

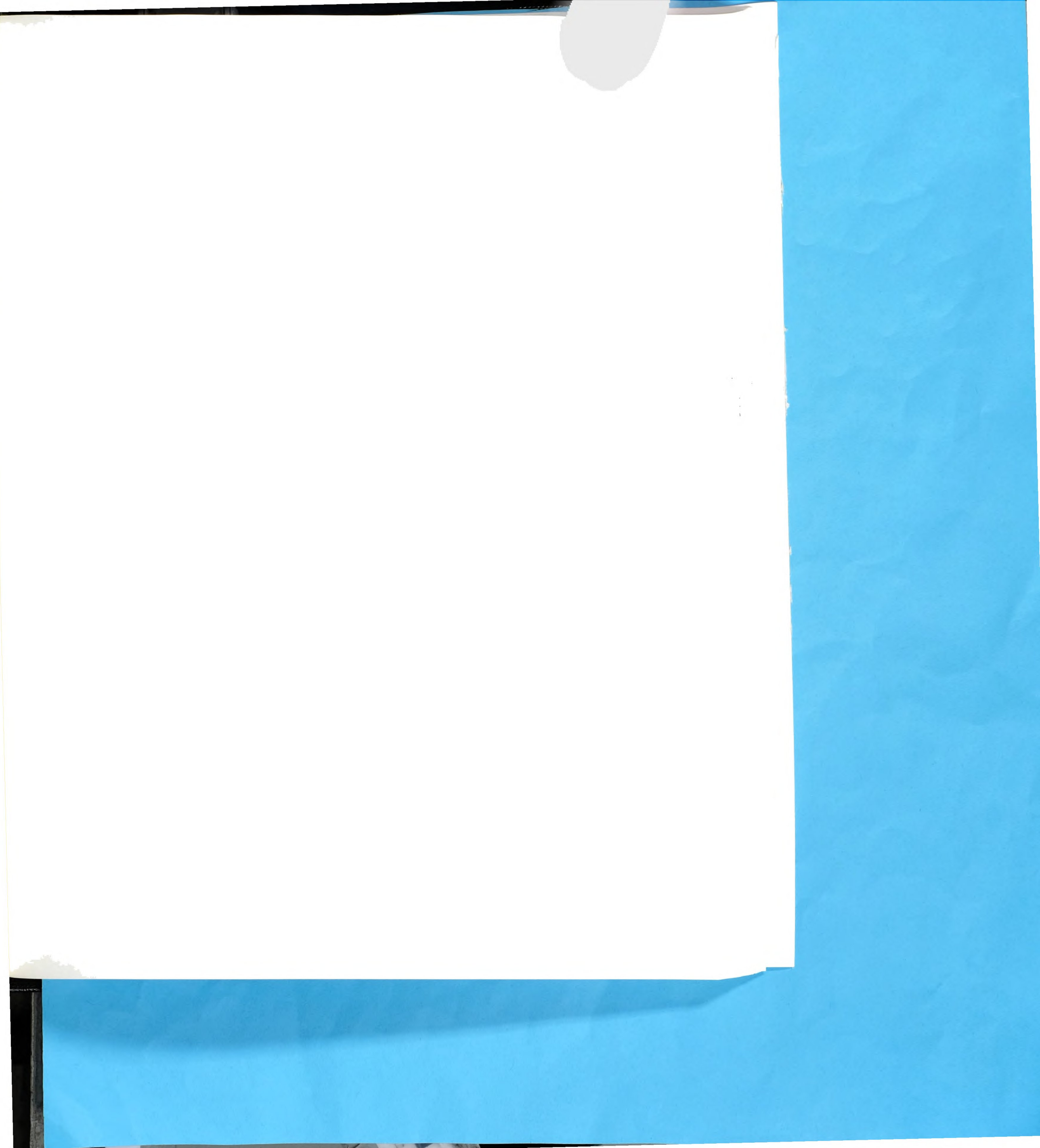

There is also one other problem associated with the fusing technique which does not have to do with the destruction of the bundle but concerns the bundle's performance. The geometric deformation of the fiber input faces causes the coupling efficiency of the deformed fibers to decrease. From figure 2.7, it is apparent that some fibers are deformed more than others. This deformation results in a reduction of light transmitted through the fiber. The output of this particular bundle had three bright fibers and four dim fibers. This nonuniformity in beam intensity could cause problems when conducting a fluid analysis study because many studies require a sheet or beam of light with uniform intensity.

The performance of this fiber bundle was somewhat disappointing after the careful consideration that went into its construction. The solution for the collimators could lie in the application of micro-lenses arranged at the fiber's output face. Meticulous detail to focal length distances and positioning is also necessary if such micro lenses are employed. For the fused technique, if burning still tends to be a problem and geometric deformation causes intensity nonuniformity, a new design must be considered. The 3M Company has designed fibers that can withstand very high power, but in order to create a bundle, the epoxy also has to be high energy absorbing. At this time, there is no epoxy that can withstand high laser pulse energy greater than 10 W/cm^2. Because of the limitations in high energy absorbing epoxy, there has not been a fiber bundle manufactured that can withstand high powered laser light. Flow visualization techniques at the MSUERL require input powers on the order of 1 W/cm^2 (this is with a laser that has a 5 cm beam diameter). When that beam is reduced to the .0075 cm^2 transmission area of the fiber bundle, the laser power becomes greater than 100 W for an area less than 1 cm^2. This energy is too great and the epoxy will burn. There also has not been a technique that is completely successful at collimating the light out of a fiber. For these reasons, a fiber bundle cannot be used with high powered laser light as a light delivery system without making significant sacrifices to the performance of the system.

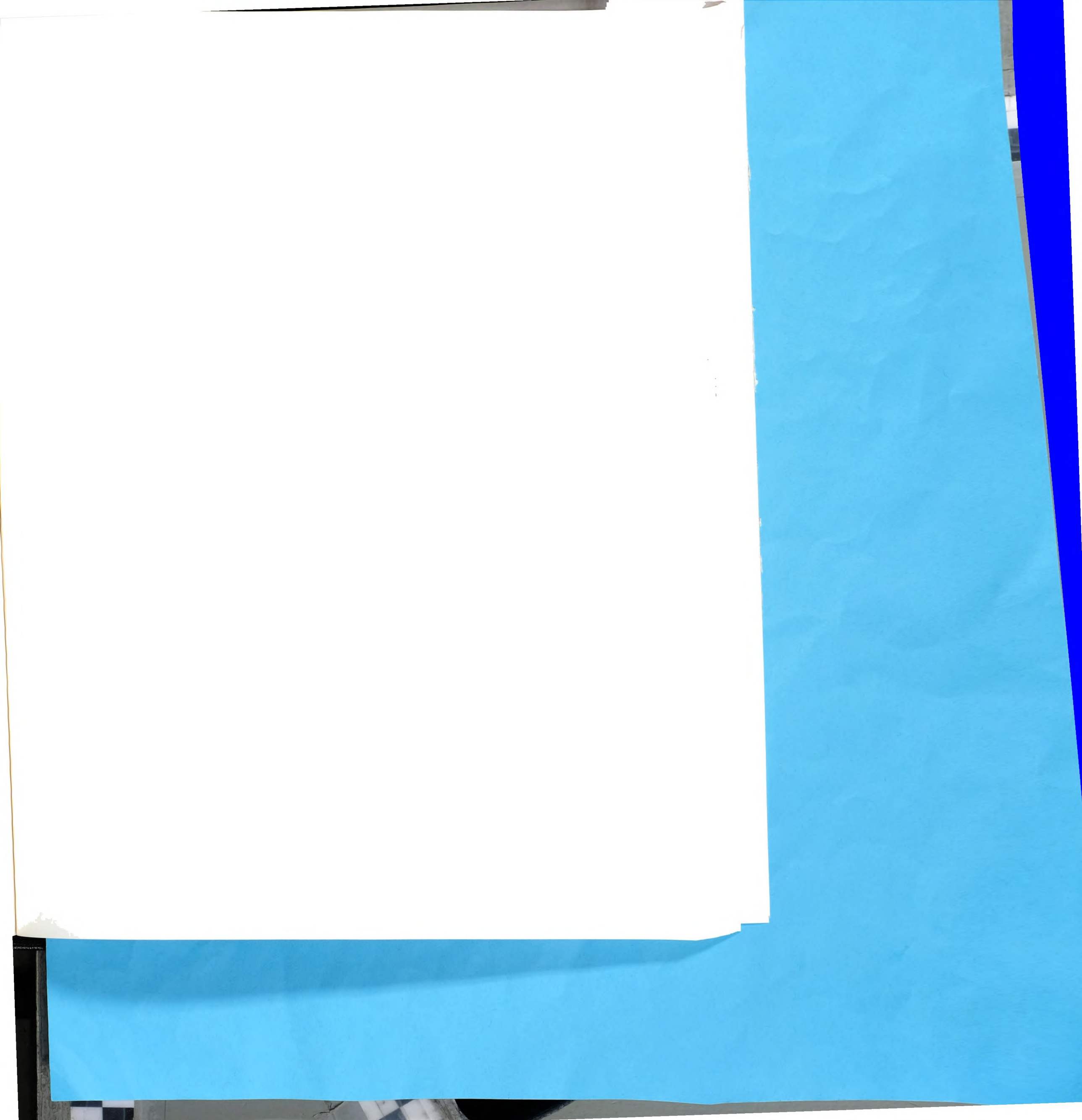

2.3 Imaging

The previously described discussion on fluid analysis has focused on a light delivery system using laser light coupled with fiber optics. However, these flow quantification studies need to not only deliver light, but they also need to image the flow field as well. Typically, flow field imaging requires a high speed camera, a 35mm camera, or a charged coupled device (CCD). These devices are used to capture the image of the particles which are following the flow of interest. Each fluid analysis method has different requirements for imaging the flow field. While some studies require high resolution, others may need speed in capturing the motion. Some systems may also be exposed to adverse temperature conditions, and others may need to reach remote locations. Whatever the case may be, the imaging system for any fluid analysis using laser light is critical to the success of the study.

At the MSUERL, numerous flow visualization studies have been conducted using a high speed camera. The main concern for this imaging system is the speed in capturing the fluid motion. When conducting flow visualization studies on internal combustion engines, it is important to study the inner chambers of the engine. This technique requires optical access for the high speed camera to film the flow features. However, it is very difficult to create an optical access inside the engine for the camera. Therefore, a remote location visualizing device is very useful.

Fiber optics are used extensively for imaging remote areas, especially in medical applications. Imaging with fiber optics is done using a coherent or image transmitting bundle. The only difference between a coherent bundle and a normal bundle or non-coherent bundle, is in the arrangement of the fibers. Both use multimode fibers, but a non-coherent bundle consists of individual fibers arranged in a random order. A non-coherent bundle is often used for light delivery applications because the randomized fiber arrangement offers the best uniformity of output light from a non-uniform input source

such as a laser. Laser light is non-uniform in the sense that the beam exhibits a guassian or bell-shaped intensity distribution and a randomized bundle somewhat evens out the non-uniform intensity. A coherent bundle on the other hand consists of individual fibers arranged in a specific order. In this type of bundle, the fibers are not randomized but arranged so that each single fiber is at the same position on the input face as on the output face. Therefore, the guassian distribution is transmitted identical to the way it entered the bundle.

For a bundle to transmit a complete image, lenses need to be placed on either end of the bundle to effectively reduce or enlarge the image to the correct transmitting and imaging size respectively. These lenses can be placed at both the input and output face of the fibers in the bundle and the protective sheath holding the fibers together can be used to enclose the lenses, making a single unit assembly. The input lens of the bundle is used to focus the image down onto the input face of the fibers and the output lens is used to increase the image from the output face to the camera or human eye. An illustration of the image transmission is shown in figure 2.12

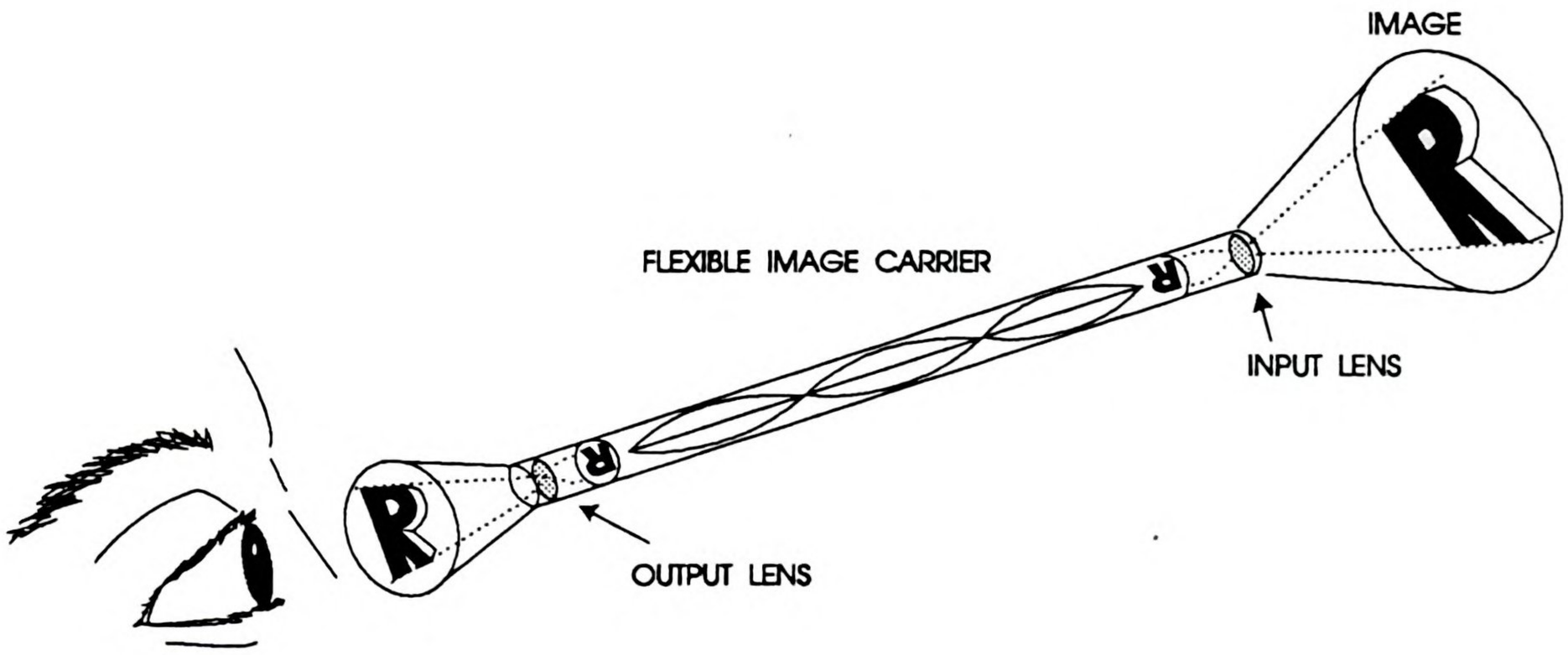

Figure 2.12 Image transmission through a flexible image carrier [10].

Notice the reduction of the image down onto the fibers at the input end of the bundle. The reduced image is then transmitted through the fibers to the output end where a second lens is used to increase the size of the image for viewing. Remember that the transmission area of the bundle is about 10 mm^2, and in order to transmit the entire image through the bundle, image size reduction and enlargement must occur. The focusing of the image onto the bundle face can be done by adjusting the position of the input lens. The input and output lenses are adjustable for ease in focusing the transmitted image. When a coherent fiber bundle comes complete with input and output lenses, it is known as an image carrier.

An image carrier divides an image up into thousands of minute parts. It then transmits each part separately within the individual fibers and recombines them at the output end. It can be thought of as a device that transports an image from one place to another. The benefits of a flexible image carrier are that it can bend, twist or "snake" its way into any remote location. It can also withstand vibrations and shock to levels equal to or greater than conventional lens/mirror systems and its resistance to corrosive environments exceeds that of most lens/mirror systems [16].

In order to assist in remote location studies at the MSUERL, a flexible Image Carrier was purchased from Olympus Corporation (see figure 2.13). The image carrier contains 36000 10μm clad optical fibers perfectly aligned for image transmission. The unit contains an adjustable focusing objective lens at the input face which can focus objects 100 mm away and beyond. The objective lens has a 40 degree field of view (FOV), and can obtain an 80 degree FOV by attaching an additional optical adaptor. The image carrier is a total of 1 meter long and has an outer protective sheath to protect it from wear [11]. A special adaptor or C-Mount was purchased to enable the image carrier to couple into the high speed camera for the filming of flow visualization. This device can also be used with other camera systems provided the compatible mounts are available to couple the image carrier to the desired systems.

With any fiber bundle system, whether light delivery or imaging, intensity losses due to light transmission through the bundle undoubtedly occur. Every bundle arrangement is different, so total light loss will vary between systems. However, the greatest light losses in a bundle are a result of both the packing fraction and the length of the bundle. The packing fraction is the ratio of the active transmitting core area of the fiber bundle to the total area of the bundle face at the light emitting or receiving end. The area that does not transmit, which includes the cladding and the interstitial spacing,

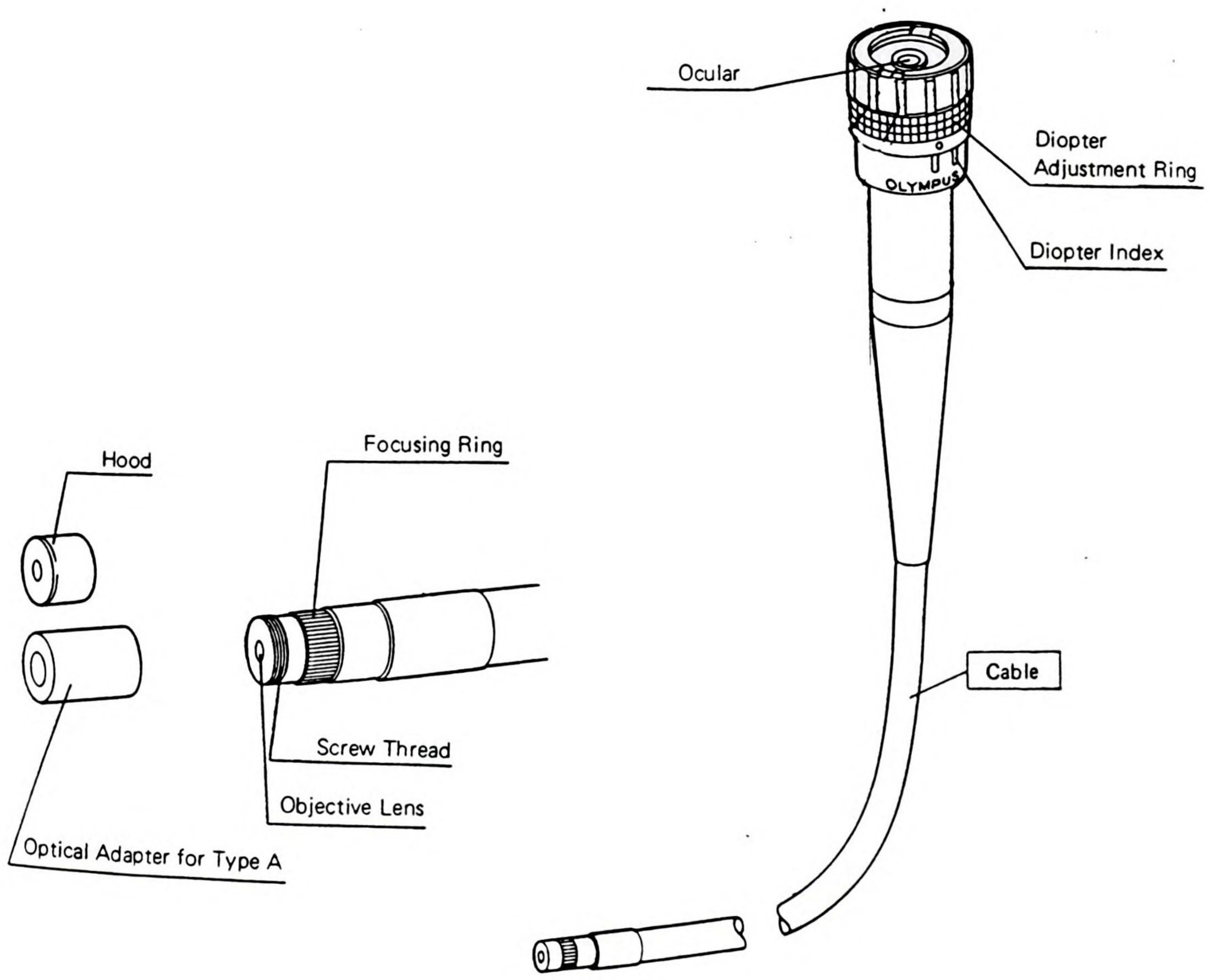

Figure 2.13 Olympus flexible image carrier [11]

should be reduced to a minimum for best transmission. The length of the bundle also causes problems because more scattering and absorption occurs proportionally to the length of the fiber. An example of transmission losses for a fiber bundle with individual fiber cores of 50 μm core glass and a refractive index of 1.625 is given below.

If all the laser light (100%) is coupled inside the acceptance cone of the fiber and the packing fraction is 85%, then the transmission after packing fraction losses is 0.85 x 1.00 or 85%. The reflective loss, known as Fresnel reflection, must also be calculated. Fresnel Reflection is due to the air glass medium through which the input and output light must travel and calculated from the expression

$$\left[(N_2 - N_1)/(N_2 + N_1)\right]^2 \qquad (2.1)$$

Here, N_1 is the refractive index of air (1.0) and N_2 the refractive index of the core glass (1.625). Therefore, the reflective loss for each face of the bundle is 5.7%. This means that transmission at each input and output surface before packing fraction losses are considered is 100% - 5.7% = 94.3%. Net transmission after input reflection and packing fraction losses is therefore 0.85 x 0.934 or 80.2%. Bulk absorption and interface scattering are responsible for a further loss of about 6% [1] per foot of bundle length or around 55% over the length of 10 feet. Net transmission after 10 feet is therefore 0.802 x 0.55 or 44%. Exit surface transmission is, as previously calculated, 93.4%, leaving a final net transmission of 0.44 x 0.934 or 41%. In other words, a 10 foot fiber bundle of the type described above will transmit only 41% of the light entering the input face.[12]

From the previous discussion, it is quite apparent that there is significant light loss associated with fiber bundles. Each bundle will vary somewhat depending on the configuration. Obviously, a shorter bundle and one with a good packing fraction (large

---

1 The 6% loss per foot of bundle is dependent on manufacturing techniques and materials used. This 6% is an average for current manufacturing techniques.

core to cladding ratio) will result in better transmission. The image carrier purchased from Olympus will transmit 70% of the incident light. Light transmission is critical to a flow visualization system utilizing a high speed camera. When the film travels at such high speeds, a great deal of light must enter the camera to expose the film. When using a fiber bundle for imaging, the associated lack of intensity through the bundle is a considerable problem for the flow visualization technique because without the proper amount of light to expose the film, the flow field will not be imaged.

Another problem that should not be over looked when using different FOV tip adaptors is that as the FOV increases, the distortion of the image also increases. This is a result of trying to transmit a larger image down onto the fiber bundle. Perimeter distortion starts to appear at a FOV greater than 40 degrees. Therefore, a compromise must be made between the desired viewing area of the flow field and the acceptable perimeter distortion.

The resolution of the image carrier is dependent upon the bundle image transmission diameter and the individual fiber core diameters. The maximum resolution for a fiber bundle can be found by

$$\text{Maximum Spatial Resolution} = d\,(1/M) \qquad (2.2)$$

where (d) is the individual fiber core diameter and (M) is the magnification factor, which is the bundle diameter divided by the object size. From equation 2.2, an illustration of the maximum spatial resolution versus the bundle diameter (with a 1 cm object size) is shown in figure 2.14. As the bundle diameter increases and the individual fiber core sizes decrease, the spatial resolution of the bundle is increased. The maximum resolution of the Olympus image carrier purchased for this study is around 10 μm when imaging a 1 cm object.

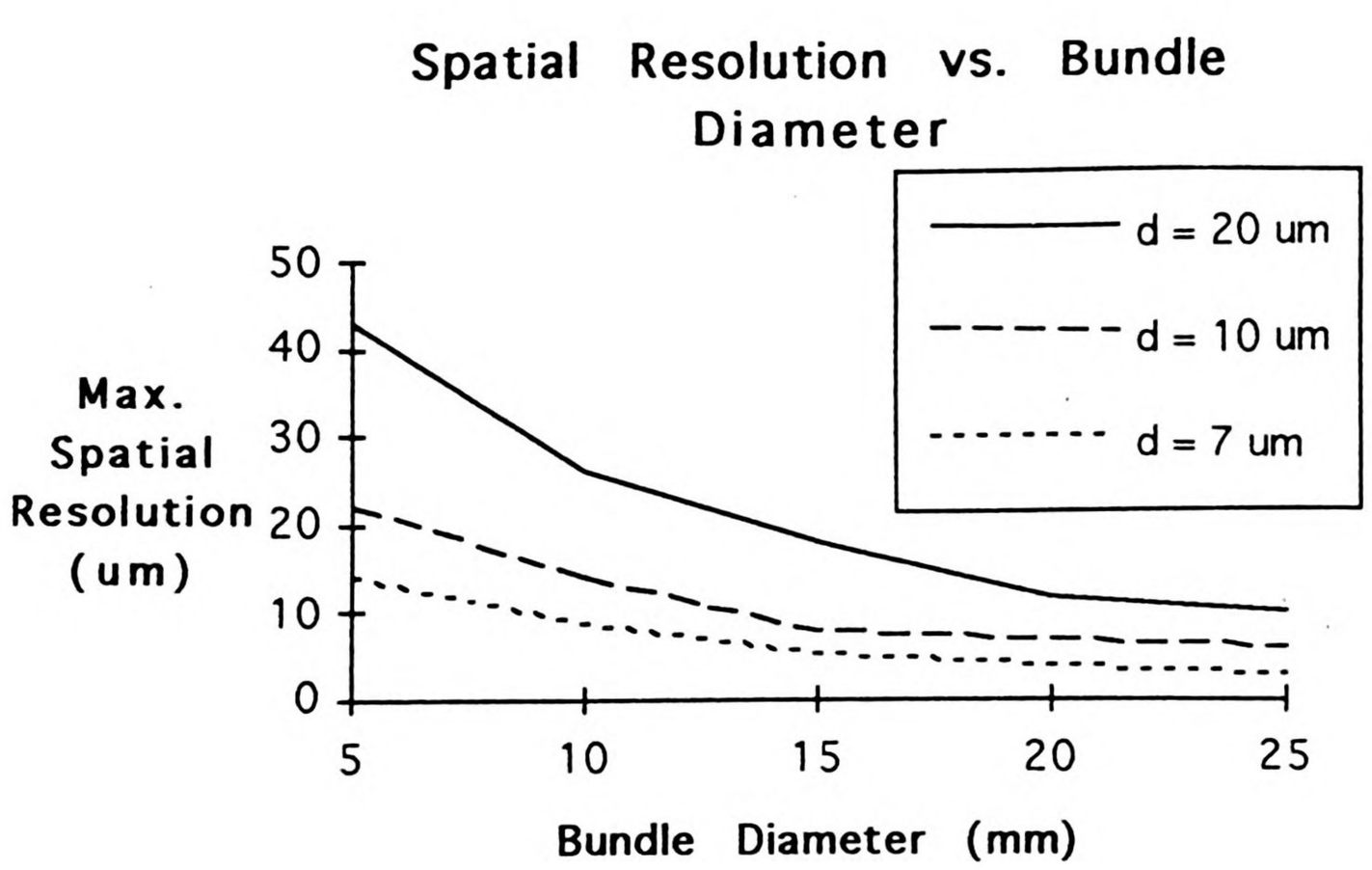

Figure 2.14 Spatial resolution versus bundle diameter for a 1 cm object.

The next section will describe the implementation of the fiber bundle as part of the imaging system in flow visualization studies. A number of these studies were conducted in internal combustion engines and the performance as well as the limitations of a fiber bundle as an image carrier will be discussed.

CHAPTER 3

TESTING APPLICATIONS IN INTERNAL COMBUSTION ENGINES

The final test for the fiber optic imaging system was to implement the image carrier into the flow visualization studies conducted at the MSUERL. Flow visualization tests using a high speed camera coupled with the image carrier were conducted in both an internal combustion engine and an air duct assembly. Some of the early tests failed because the light intensity transmitted through the image carrier was insufficient to expose the photographic film. These failures will be described, as well as the successful testing in both a steady state and a motored engine. The final test procedure in the motored engine will be described in complete detail along with a discussion on the overall performance of the image carrier.

3.1 Testing in a Rotary Engine

The implementation of the image carrier was designed to enhance the current flow visualization techniques. Enhancement came in the form of remote location imaging and in a reduction of the size of the transparent window used for viewing the flow field. At the time of the initial image carrier testing, studies were being conducted on the high pressure fuel injection system of a Rotary engine assembly. A flow visualization test on the fuel spray development had been conducted using two large transparent windows in the engine housing. Figure 3.1 illustrates the optical arrangement for the test. A sheet of laser light was delivered through the top Plexiglass window, and the fuel spray was imaged by the high speed camera through the side sapphire window.

For the newly designed test using the image carrier, the large top Plexiglass window was replaced by a small threaded insert about 1 inch in diameter with a

Plexiglass face at the bottom. The image carrier was placed into the insert and a top view of the fuel spray was imaged. The sheet of laser light was, in this case, delivered

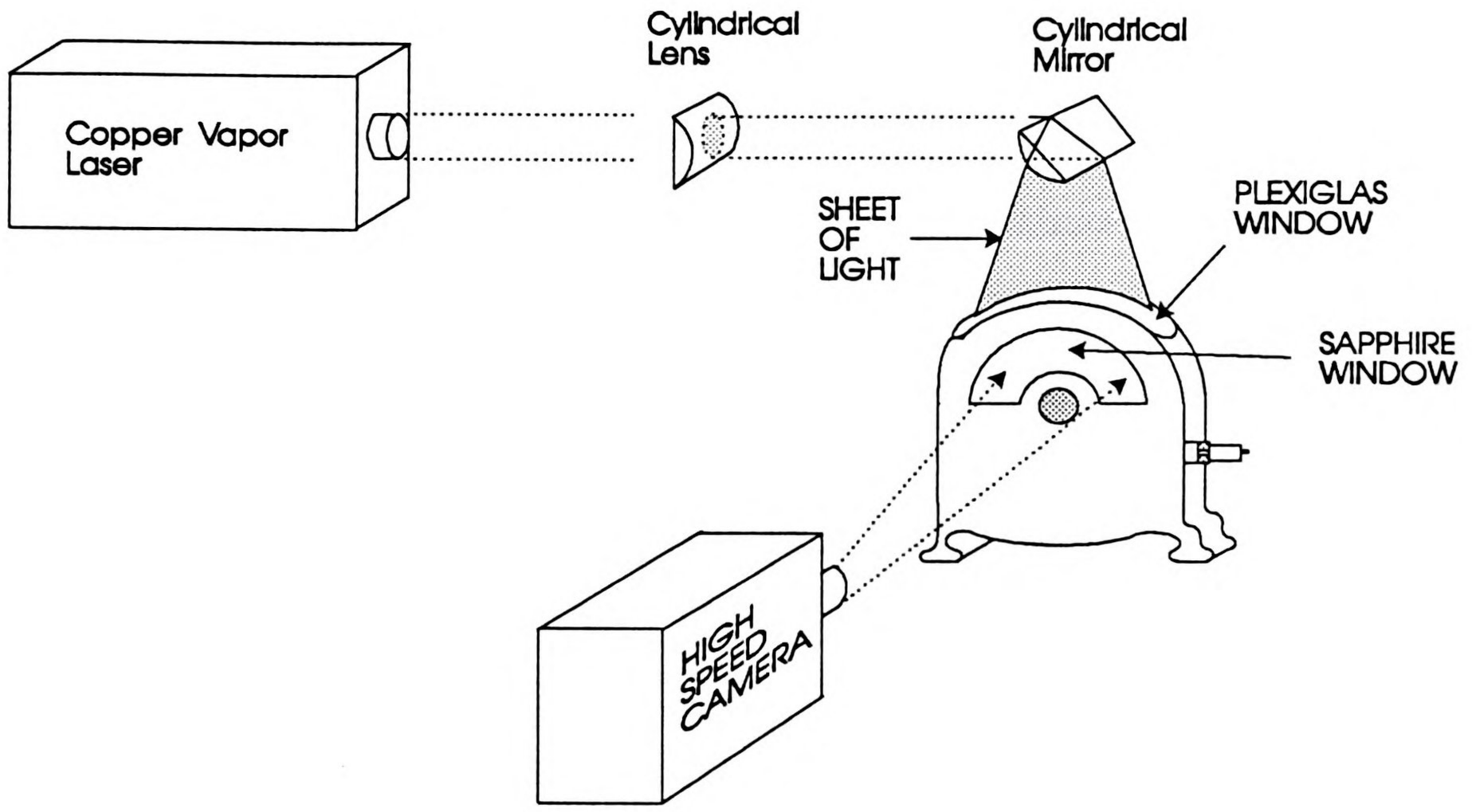

Figure 3.1 Flow visualization test using transport windows for optical imaging.

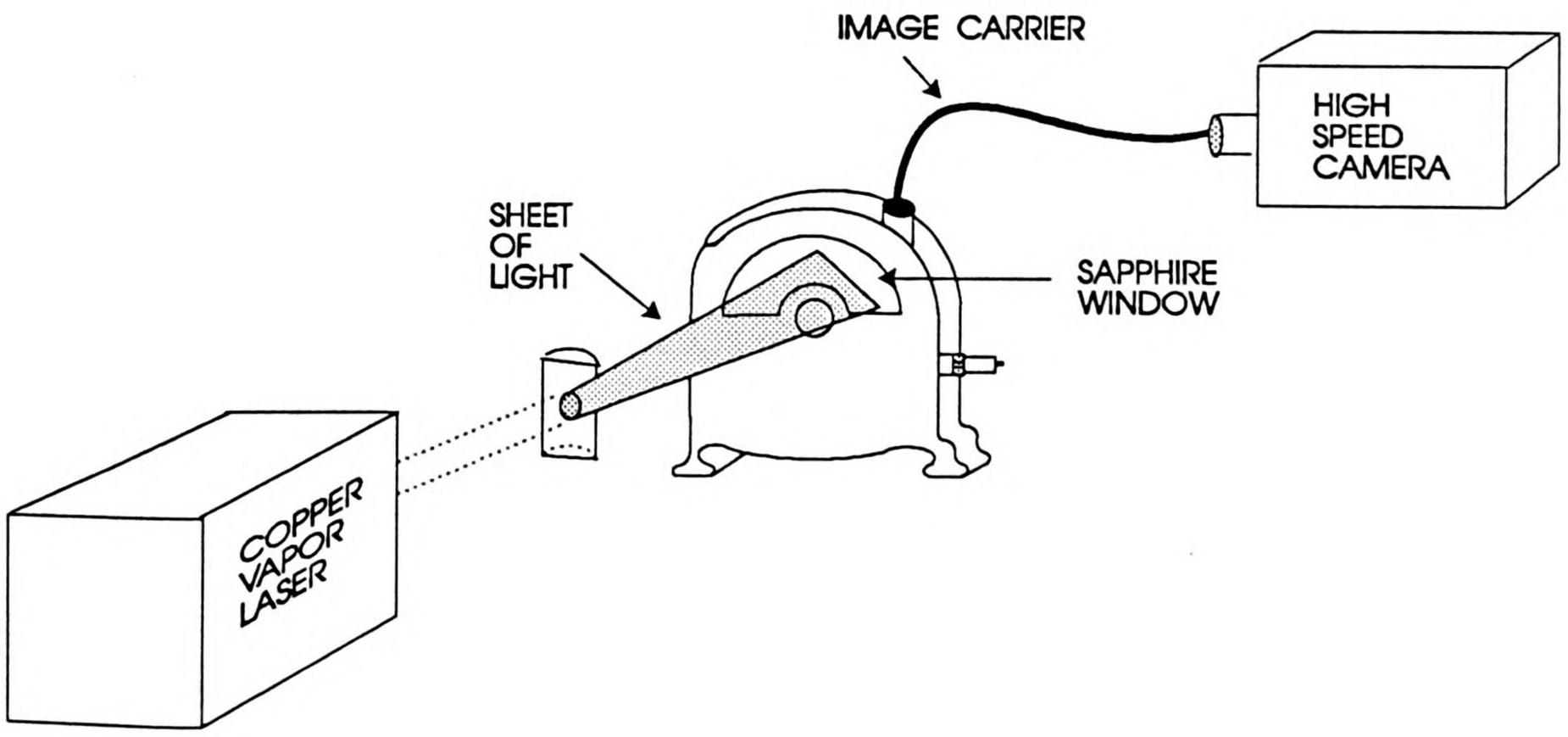

Figure 3.2 Flow visualization using the image carrier for optical imaging.

through the side sapphire window (see figure 3.2). By using the threaded insert with the image carrier instead of the top Plexiglass window, the size of the transparent window was reduced by 90%.

A comparison of the two films was made to see what type of image quality the fiber optic image carrier transmitted. However, no visible particles from the flow pattern appeared on the film because the intensity of the laser light transmitted through the image carrier was insufficient to expose the film. Even though there wasn't enough light to image the entire flow field, the film did show some small, dim fragments of the fuel spray, leading to the conclusion that the test procedure was conducted correctly. This test was somewhat of a complicated test configuration, which in turn may have contributed to the lack of transmitted light. Therefore, the next test was simplified and designed to refine test parameters effecting the light intensity entering the high speed camera.

The test parameters examined which controlled the light intensity were the light scattering ability of the seed particles in the flow field and the placement of the image carrier in relation to the light scattering direction of the particles. Different particles that are used to seed the flow tend to scatter the light at various intensity levels, and it is important to use a particle with good light scattering ability. It is also important to view the light scatter at the proper angle. When laser light scatters off particles, the best scatter intensity is located downstream and slightly off axis of the particle. This is known as forward scatter. When the particle is very small ($< 0.1\ \mu m$) as in figure 3.3a, there is an intensity maximum in the forward direction ($\theta=0$) and in the reverse direction ($\theta=180$), and there is a minimum in the plane of symmetry ($\theta=90$). As the radius of the particle increases (to the size of the seed particles), more light is scattered in the forward direction (see figure 3.3b). This light scattering principle is known as the Mie scattering effect [15]. Therefore, the best position for viewing the flow field is near positions A and B, at about 20 or 30 degrees from the incident beam. These positions

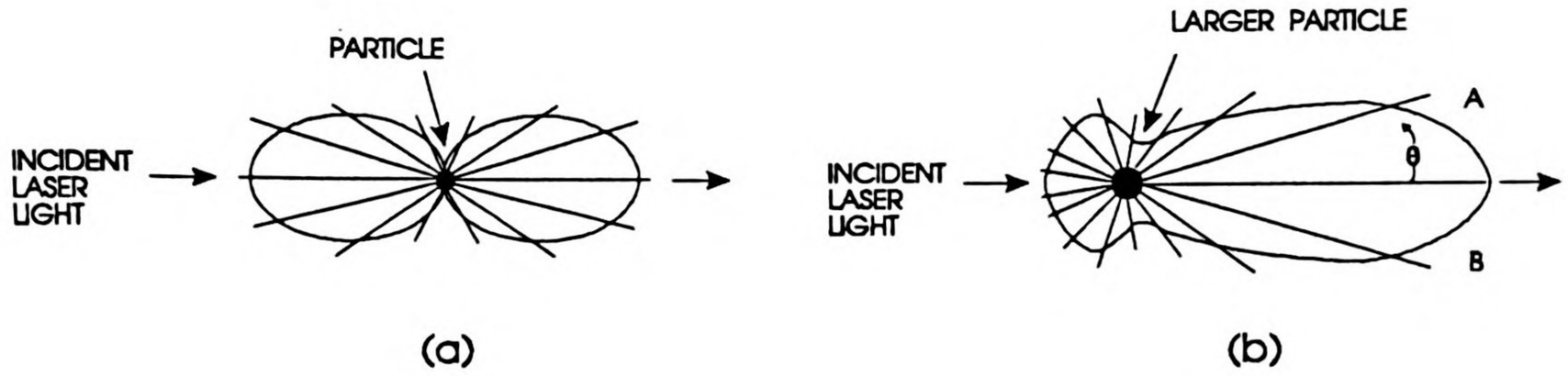

Figure 3.3 Polar diagram illustrating the relative intensity magnitudes from particle scatter on different size particles.

offer sufficient intensity without being too close to the direct path of the incident beam.

3.2 Testing in an Air Duct Assembly

To test the above mentioned theories, another flow visualization test was conducted in an air duct assembly. In this study, the air duct assembly was seeded with smoke particles. The study was designed to quantify the increase in the scattered light by trying two different positions for the image carrier. The first position was perpendicular to the sheet of light, or 90 degrees from the incident beam. The second position was placed for maximum scatter intensity, near the vicinity of points A or B in figure 3.3b. This position was about 30 degrees from the incident beam. The first flow visualization test filmed the flow field at 5000 fps with the image carrier placed at the 90 degree position. The second test was filmed in two parts at 500 fps. The first part of the film placed the image carrier at the 90 degree position, and the second half of the film placed the image carrier at the 30 degree position.

The area of interest to be filmed was the bypass located in the rear of the conical assembly. It was important to visualize the pattern of the flow field around the bypass to see whether the flow appeared laminar or turbulent when entering the bypass. Smoke was entrained into the assembly as it passed through the filter toward the bypass. The test

configuration is shown in figure 3.4. The first film with the perpendicular viewing angle and the 5000 fps did not image the flow field. Again, not enough laser light entered the camera to expose the film. However, the second film at 500 fps did expose the film and

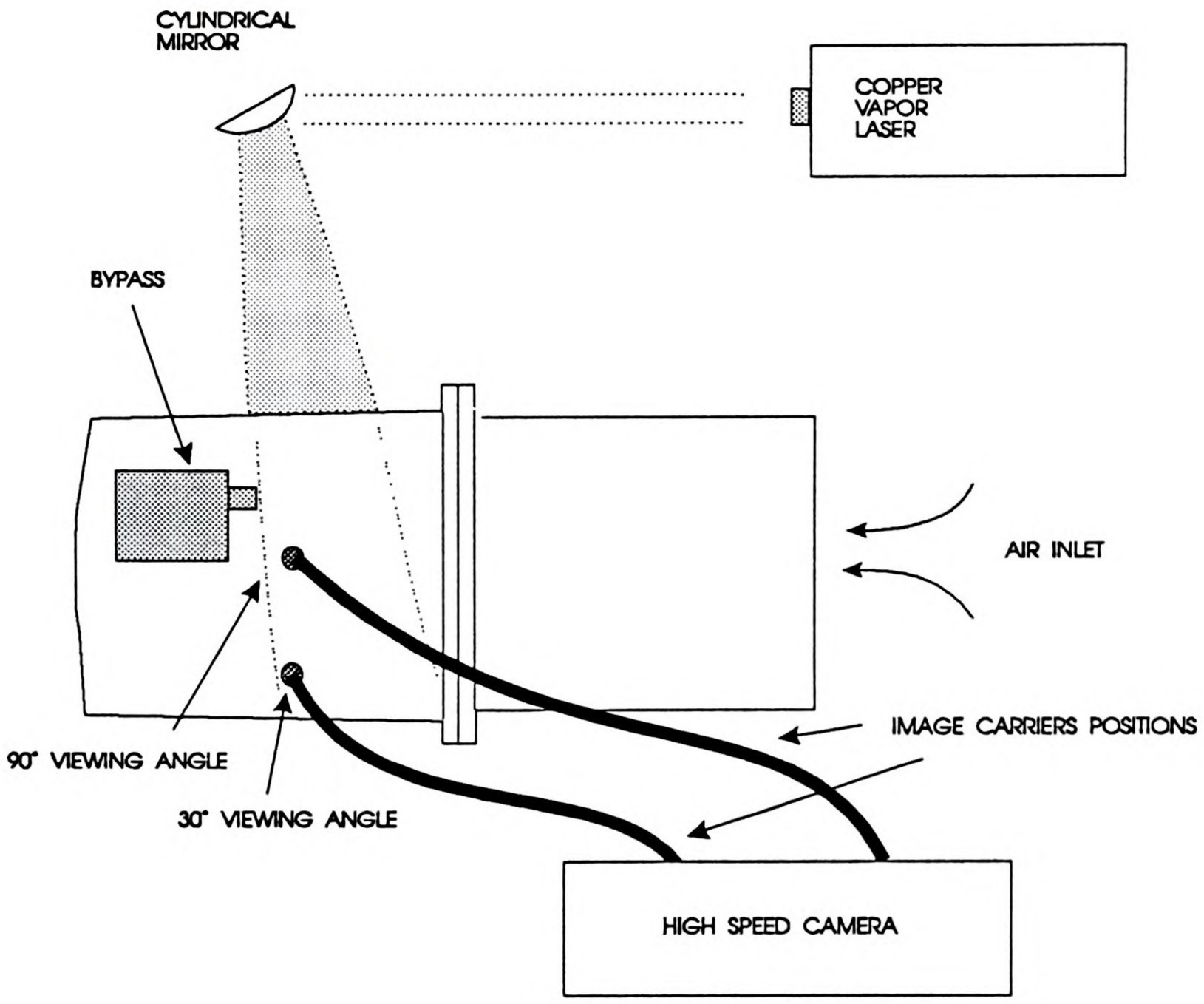

Figure 3.4 Air duct assembly and test configuration.

allow a visualize of the flow field. This was to be expected because the slow rate of the film allowed more light into the camera to expose the film. However, at this slow speed, too much of the flow field was missing in between frames, and the individual particles could not be tracked. The purpose of the film was to show the light intensity increase with the different image carrier angles. The second part of the film at the greater scatter angle showed a marked improvement in the light intensity entering the camera. The

smoke streamlines were brighter and more streamlines were visible. Even though the first test did not show the results that were anticipated, the second test showed results which would be expected according to Mie scattering theory and gave good insight into the control of the test parameters for the design of future tests. The two different imaging angle positions are illustrated in figure 3.5. An increase in intensity can be seen by viewing from the top left to bottom right; where photos c and d represent the better light scattering angle.

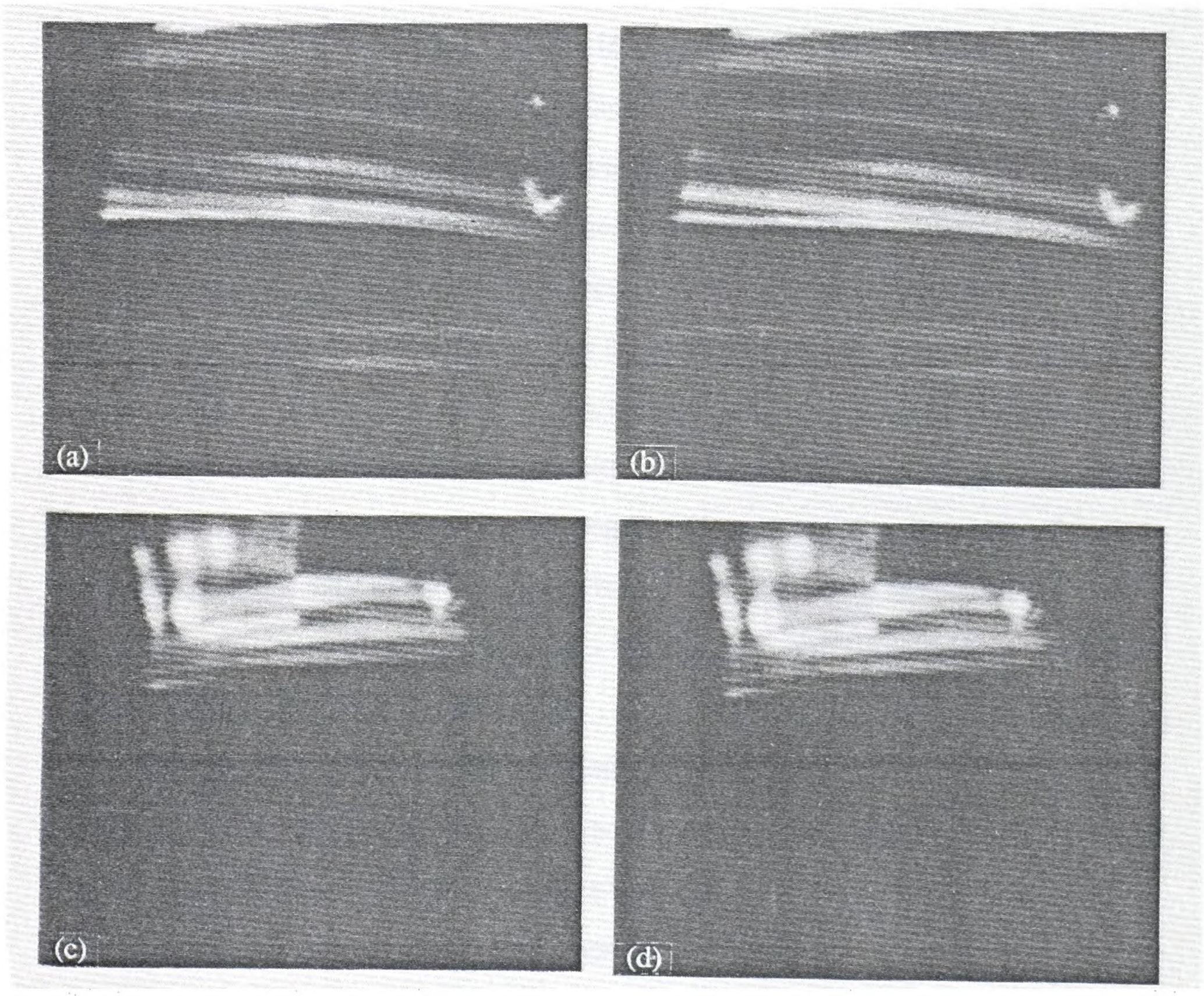

Figure 3.5 Successive frames illustrating Mie scattering angles in an air duct assembly.

3.3 Flow Visualization in a Steady State Cylinder Head

The valuable information gained from the previous tests was implemented into the design of a new test on a steady state 2.2 L Cylinder head, and 3.5 L motored engine. Both tests were conducted with microballoon particles and a new particle mixing device. This mixer, designed at MSUERL, as well as some successful testing will be described in further detail in appendix A.

Using the particle mixing device for the microballoons, a new flow visualization test was conducted on a 2.2 Liter Cylinder Head. A previous flow visualization test had been conducted in the radial plane of the cylinder [14]. This test was then repeated using the image carrier and a comparison of the two results was to be conducted. The new test configuration is shown in figure 3.6. This test was conducted using a planer but slightly diverging sheet of laser light from the copper vapor laser. The light sheet entered the cylinder in the radial plane about 1.5 inches from the intake valve. The intake valve was opened about 0.5 inches and the flow rate through the cylinder was 38 cubic feet per minute (cfm). The output end of the image carrier was mounted to the high speed camera and the input end, with the 80 degree FOV tip adapter, was inserted into a hollowed out spark plug housing and used for viewing the flow field through the actual spark plug hole. The high speed camera was synchronized to the laser pulse and set to a filming speed of 5000 fps.

The high speed film from this new modified test was inconclusive since only a dim image of the flow pattern was exposed on the film. However, the dim image meant that the test nearly obtained the correct amount of light, so the next step was to enhance the collection of light into the high speed camera. This was done by both narrowing the planer sheet of light from the laser, which increased it's intensity, and by using the 40 degree FOV lens on the image carrier. The 40 degree tip was used because it has a greater light collecting ability associated with its shorter focal length lens assembly.

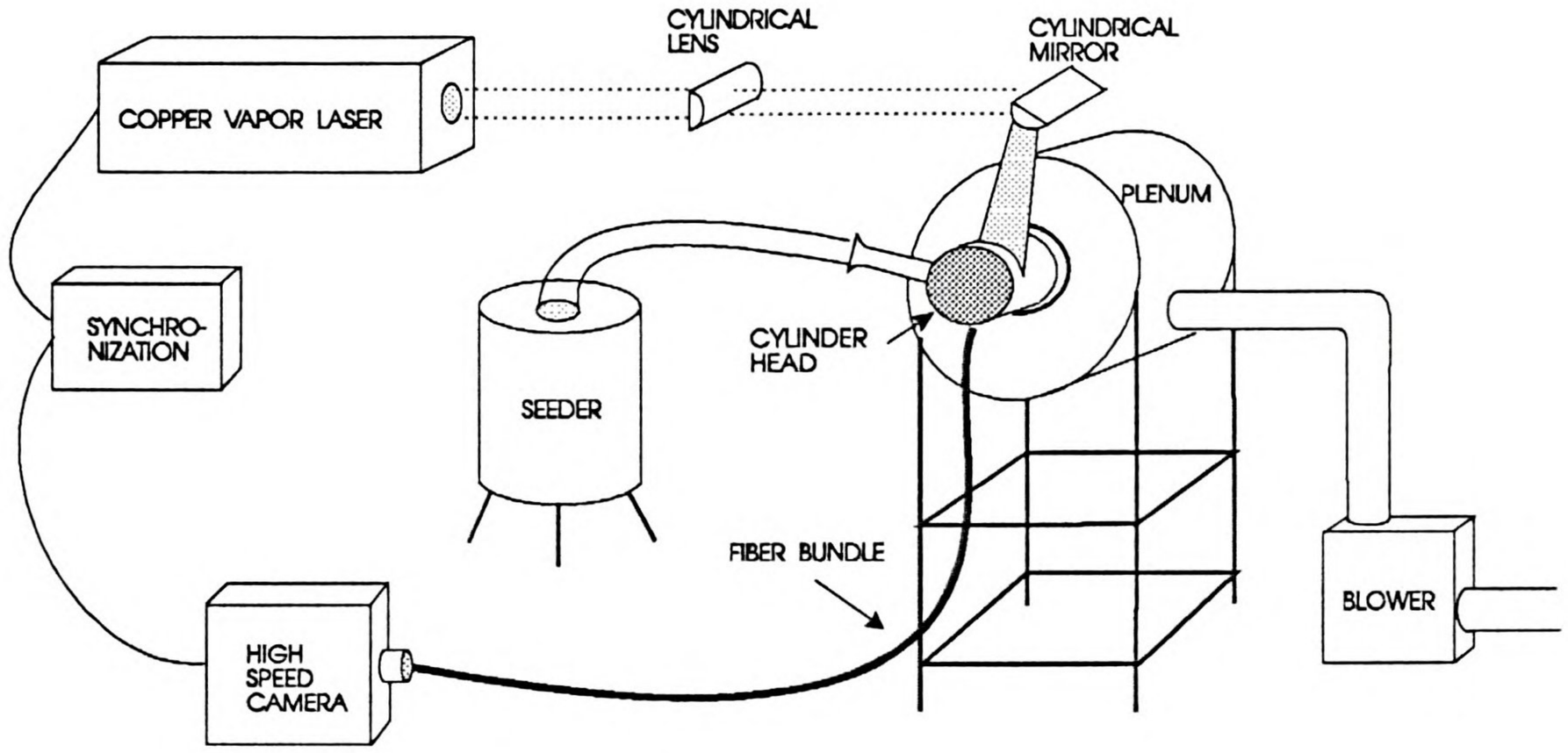

Figure 3.6 Schematic showing the experimental setup for flow visualization in the steady state 2.2L cylinder head.

With these optical system modifications, another imaging test was conducted. This new test produced conclusive results showing flow patterns on the high speed film. By stepping through the film, associated swirl and turbulence could be tracked from one frame to the next. Even though this was the first test that showed particle motion, there were several parameters which needed to be modified. When using the 40 degree FOV tip, only part of the cylinder (about 30%) was visible. For flow visualization, it is important to image the entire plane of interest to track related influences and causes of flow field motion. Therefore, for the next test which took place in the motored engine, the 80 degree FOV tip adaptor was used to collect more information. When using the 80 degree FOV adaptor, the sheet of light then needs to be spread wider than the 2.5 inches used in the previous test. The drawbacks of changing these parameters (the width of the sheet of light and the 80 degree FOV) are that both changes reduce the amount of light through the image carrier.

3.4 Flow Visualization in a Motored Engine

With the success of the last flow visualization test in the steady state 2.2 liter cylinder head, a new study was conducted under similar conditions in a motored 3.5 liter cylinder head.

A series of three tests were taken in the radial plane near the upper end of the cylinder head assembly. To visualize this plane, the image carrier was placed at the top of the cylinder head in the spark plug position. To design a positioner for the image carrier, a spark plug was bored out and the inner diameter enlarged to allow the image carrier to fit snuggly. A schematic of the new spark plug holder is shown in figure 3.7. A Plexiglass face was inserted into the bottom of the spark plug to protect the image carrier from adverse test conditions and to prevent leakages. Pressures in the engine may

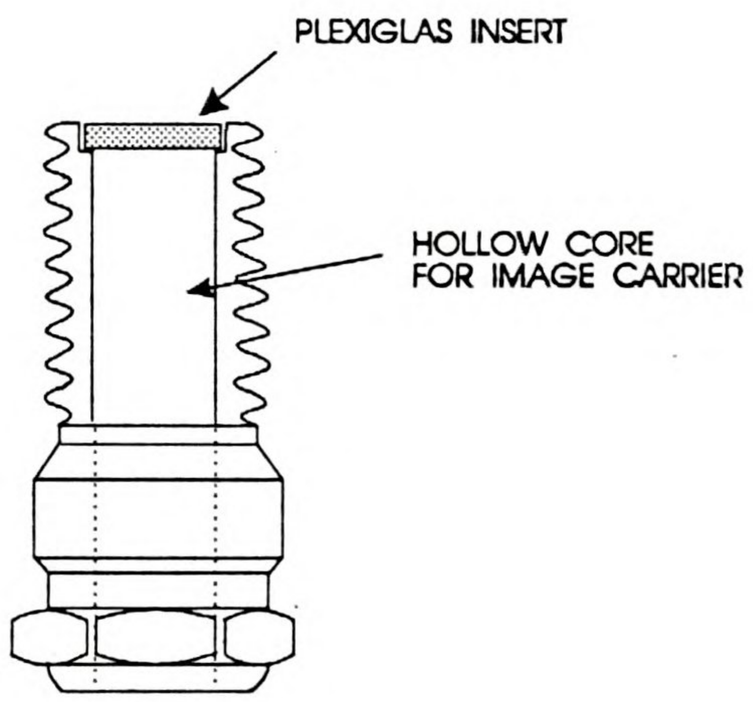

Figure 3.7 Spark plug holder for image carrier.

reach 230 psi and temperatures may reach 100 C. Therefore, the Plexiglass was positioned securely in place to withstand these test conditions while allowing a clear view of the flow field.

For the experiment, the copper vapor laser (CVL) was configured to pulse at 5 kHz with 20 Watts of average power. The pulse energy was 8 mJ and the pulse duration was 30 ns. The NAC high speed camera operated at 5000 fps, and 200 feet of Kodak high speed negative film was utilized for each test. The first test used the mc-08 C-mount camera adaptor and the second test used the mc-05 camera adaptor. Both of these tests used the 80 degree FOV tip adaptor. The third test used the mc-05 camera adaptor and the 40 degree FOV tip for viewing the flow field. The mc-08 adaptor allows the transmitted image to expose 80% of a single frame on the high speed film, and the mc-05 adaptor allows an exposure of 50% of the frame. Theoretically, the mc-05 adaptor should increase the intensity of the image on the film by about 25-30% because the image is not spread out as much on the film. The 3.5 liter engine was motored to 810 rpm with a flow rate of 9 cfm. The engine had a bore of 96 mm, an 8 mm stroke length and a maximum valve lift of 9 mm. The microballoon seeder was attached to the intake port and a blower was used to ventilate the exhaust. The experimental setup is shown in figure 3.8. For all three tests, the seeder was filled with approximately 12 oz. of microballoons. With an engine flow rate of 9 cfm, the concentration of seed particles to air was estimated to be less than 2% by volume. Detailed calculations for particle concentration are shown in Appendix B.

To conduct the test, the beam from the CVL was expanded into a sheet of light by a cylindrical lens, and was then directed into the engine by a series of mirrors. The sheet of light was 10 cm wide and about 2.5 mm thick. After proper orientation of the laser beam, the synchronization between the high speed camera and the CVL was checked. This was done by reflecting some of the laser light into the timing gears of the NAC Camera. When the high speed camera reached a speed of 5000 fps, the action of the timing tabs was observed. Synchronization occurred when the tabs were aligned with the timing mark. At this point, the 80 degree tip adaptor on the image carrier was focused and placed in the spark plug holder. With the 80 degree FOV, about 75% of the cylinder

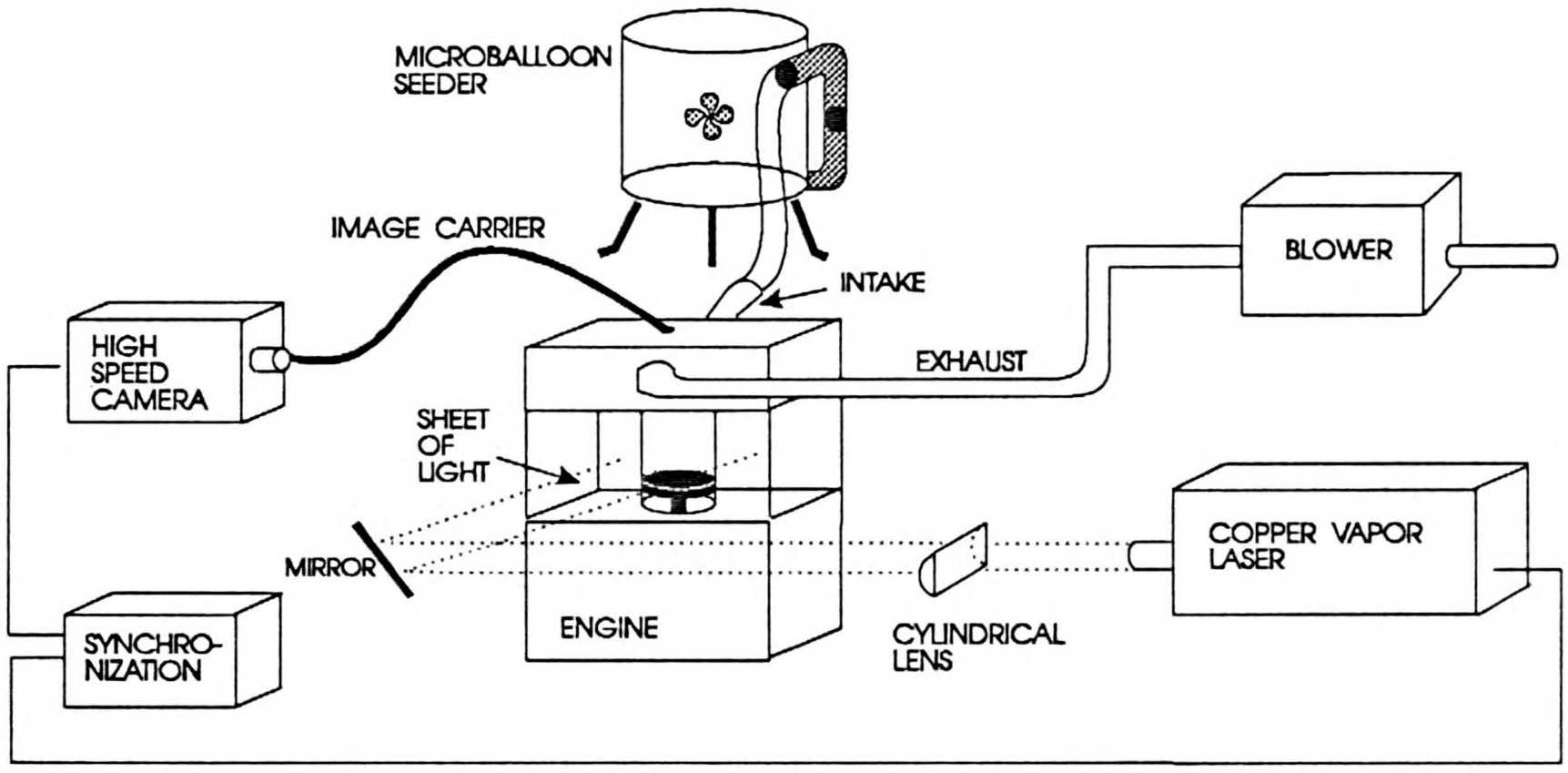

Figure 3.8 Motored engine experimental setup.

was visualized. The 40 degree adaptor, for the third test, imaged around 35% of the flow field. The other end of the image carrier was then attached to the high speed camera by either the mc-08 or the mc-05 C-mount adaptor, depending on the configuration used.

Just before exposing the film, the blower was turned on and the engine started. Microballoons were placed in the seeder with the throttle in the closed position and the shutter of the laser was opened to allow the sheet of light to passed through the cylinder. The throttle of the seeder was then opened and the camera was started. The duration of the filming was 2 seconds.

The results of the film using the mc-08 adaptor were not as bright as the film with the mc-05 adaptor, proving that more intensity occurs with the smaller image camera adaptor. This smaller adaptor allows a more concentrated beam to expose the film. It is the same principle when using a flashlight. If the beam is reduced from 80 degrees to 50 degrees, the intensity increases. The result of the third film showed that the 40 degree FOV transmits more light than the 80 degree FOV. Therefore, this third case illustrates the best case for the light transmitting ability of the image carrier.

Separate successive frames from the three films are shown in figures 3.9 through 3.11, for comparison of the light transmitting ability. Each film was taken at 5000 fps and the exposure time for each frame was 20 ns. Figure 3.9 shows the first test using the mc-08 camera adaptor and the 80 FOV degree tip adaptor. The six frames show the intake cycle as the piston moves down, starting at a piston crank angle position of 63 degrees, and moving 0.5 degrees for each additional frame. The elapsed time for each successive frame is shown in the lower left corner of the frame. A bright spot appears near the top of each picture due to the reflection of the laser light off the quartz cylinder. There is also another bright spot in the center of the picture due to a reflection off a slightly raised surface on the piston. From these results, it is apparent that most of the flow field is not visible.

The second test conducted used the 80 FOV degree tip adaptor and the mc-05 camera adaptor. Successive frames from the flow visualization film are illustrated in figure 3.10. The only parameter changed between the two films was the camera adaptor. It appears that more of the flow field is visible in the second test. By using the mc-05 camera adaptor, an additional 20 -25% more light intensity entered the film.

The last test, shown in figure 3.11, used a 40 degree FOV tip adaptor and the mc-05 camera adaptor. The sheet of laser light was also reduced to about 2.5 inches, where in the two previous test, the sheet was spread to about 6 inches. In this film, virtually all of the flow field was visible. Again, six frames illustrating the engine intake are shown, but these frames show the swirling motion in the center of the cylinder which was not visible in the two previous films. This last test used the optimum test configuration for capturing light intensity on the film.

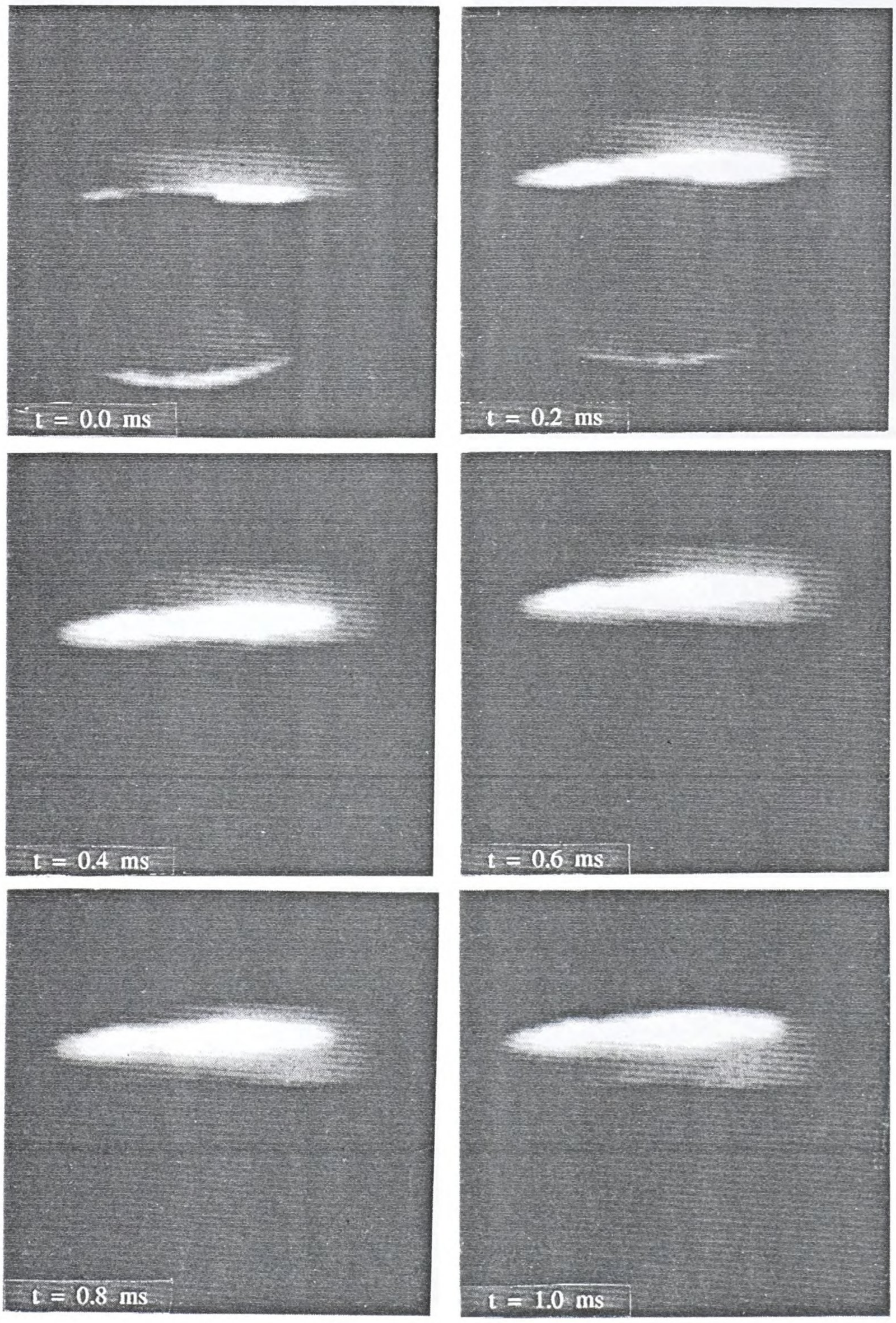

Figure 3.9 Successive frames of the motored engine using the 80 degree FOV and the mc-08 camera adaptor. The exposure time for each frame is 20 ns.

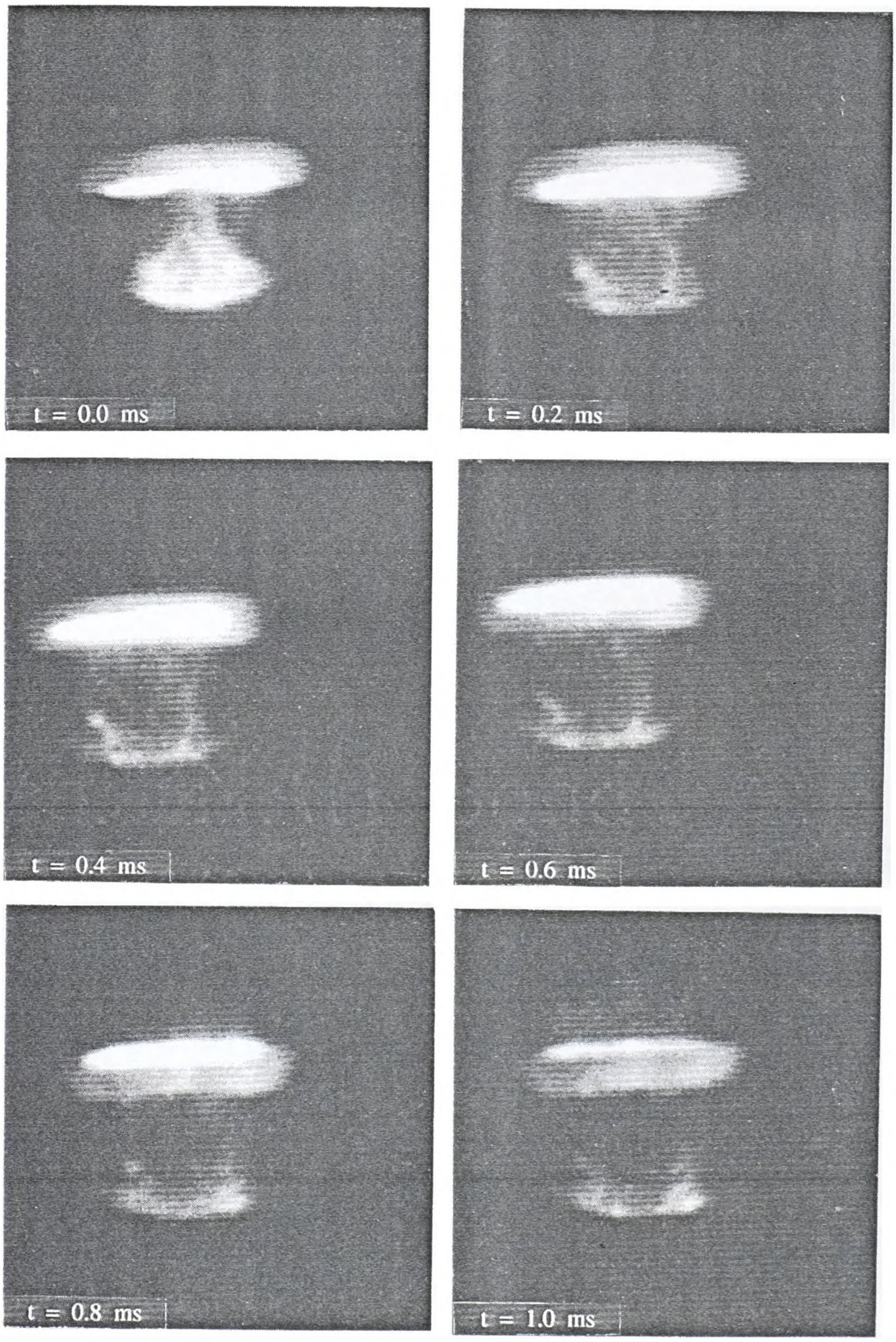

Figure 3.10 Successive frames of the motored engine using the 80 degree FOV and the mc-05 camera adaptor. The exposure time for each frame is 20 ns.

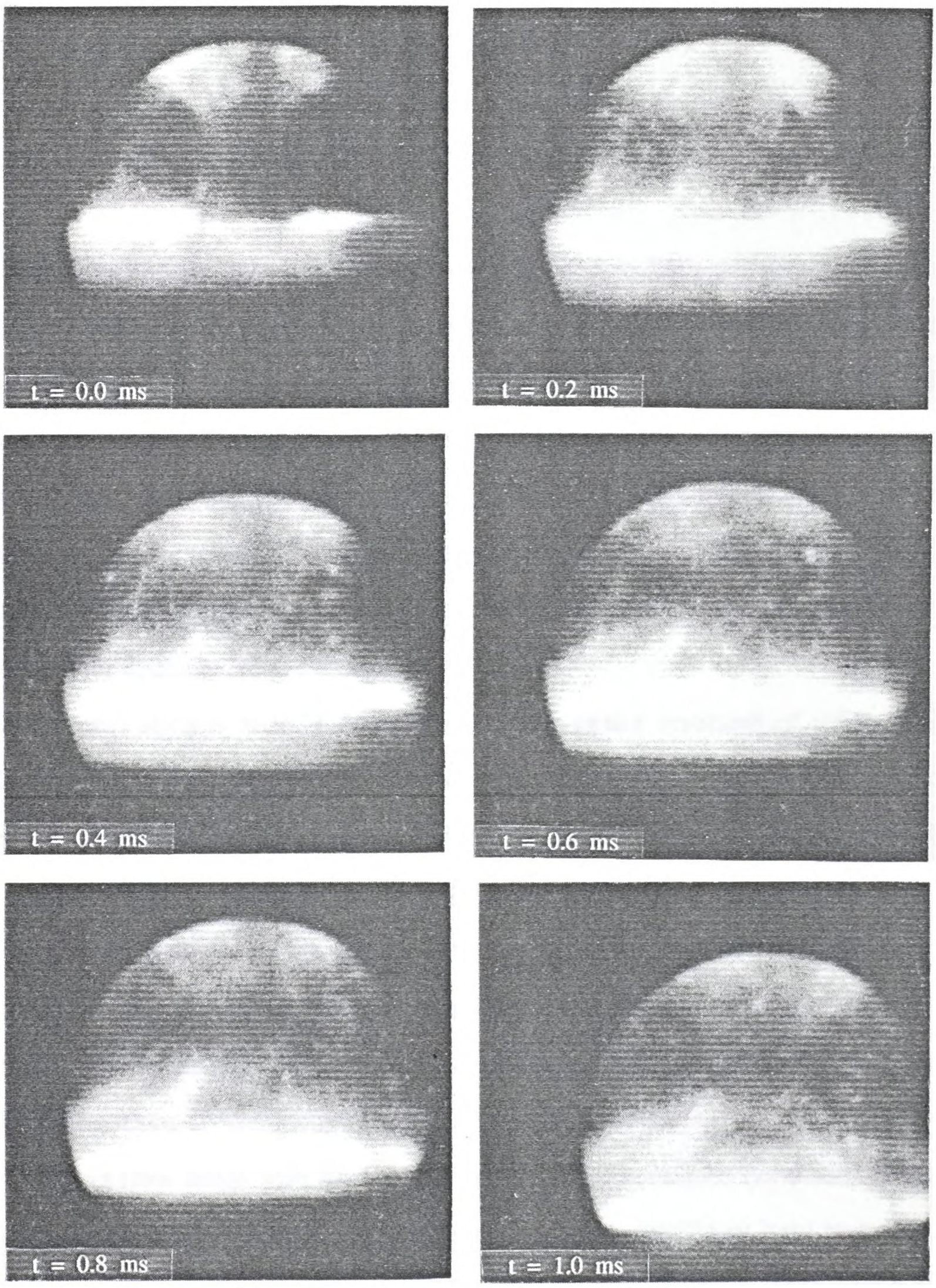

Figure 3.11 Successive frames of the motored engine using the 40 degree FOV and the mc-05 camera adaptor. The exposure time for each frame is 20 ns.

CHAPTER 4

SUMMARY AND CONCLUSIONS

The characteristic behavior of fiber optics applied to light delivery and imaging systems for fluid analysis has been described throughout this study. Research consisted of trying to enhance conventional light delivery systems with fiber optics. The enhancement was achieved by delivery a sheet of light through a single fiber optic cable. This was done to eliminate the optical access windows associated with the conventional light delivery systems. However, creating the sheet of light with a single fiber did not reduce the optical access window because of the complicated lens system needed at the end of the fiber to create the sheet of light.

The next attempt at light delivery with fiber optics consisted of using a fiber bundle to deliver a grid pattern of collimated light beams into a test site. Coupling high power laser light into a fiber bundle causes the interstitial spacing between the individual fiber cores to burn. Therefore, a special fused bundle was designed and built to withstand the high power of the laser. However, the collimating lenses on the output face of the bundle failed to collimate the light effectively, and the geometric deformation of the fiber cores from the fusing process caused non-uniform intensity of light through the fibers. Therefore, further study of the bundle was not conducted.

Imaging flow fields with fiber optics proved more beneficial because flow fields can be imaged with commercial image carriers. However, significant light losses occur. Numerous tests were conducted to study different light intensity parameters. Tests in an air duct assembly illustrated the Mie scattering effect associated with particle scatter, and tests in a motored engine evaluated field of view and camera adaptors to see which parameters enhanced the light collecting ability of the image carrier. From the research and experimentation conducted, the following remarks can be made.

1. For light delivery systems, fiber bundle technology is not advanced enough for applications involving fluid studies using high power lasers. Standard fiber bundles will burn at the face of the fiber with power inputs greater than 10 W/cm^2. Special fused bundles can be designed, but these bundles may burn as well. It would be very difficult to determine where the fused bundle failed since failure could occur anywhere in the vicinity of the fused section.

2. For the flow visualization technique, where a sheet of light is needed to image the flow field, single fibers offer a benefit over conventional optics in terms of remote location light delivery. However, a single fiber does not reduce the optical access window needed for light delivery into the test site, and the quality of the light sheet is sacrificed because of the non-uniform intensity associated with multimode fibers.

3. GRIN Lenses mounted to individual fibers do not collimate light effectively for current fluid quantification techniques, such as LIPA.

4. For imaging remote location flow fields, commercial image carriers can be used for high speed flow visualization studies. However, when doing high speed flow visualizations, these image carriers lose a large amount of light intensity when transmitting the image. The total light loss depends on a number of different parameters such as field of view, packing fraction and camera adaptors. The feasibility of using such image carriers depends on the unique characteristics of each experiment.

5. Image carriers also have limitations in their field of view during testing. Some image carriers will image as large as 120 degrees, however, beyond a 60 degree

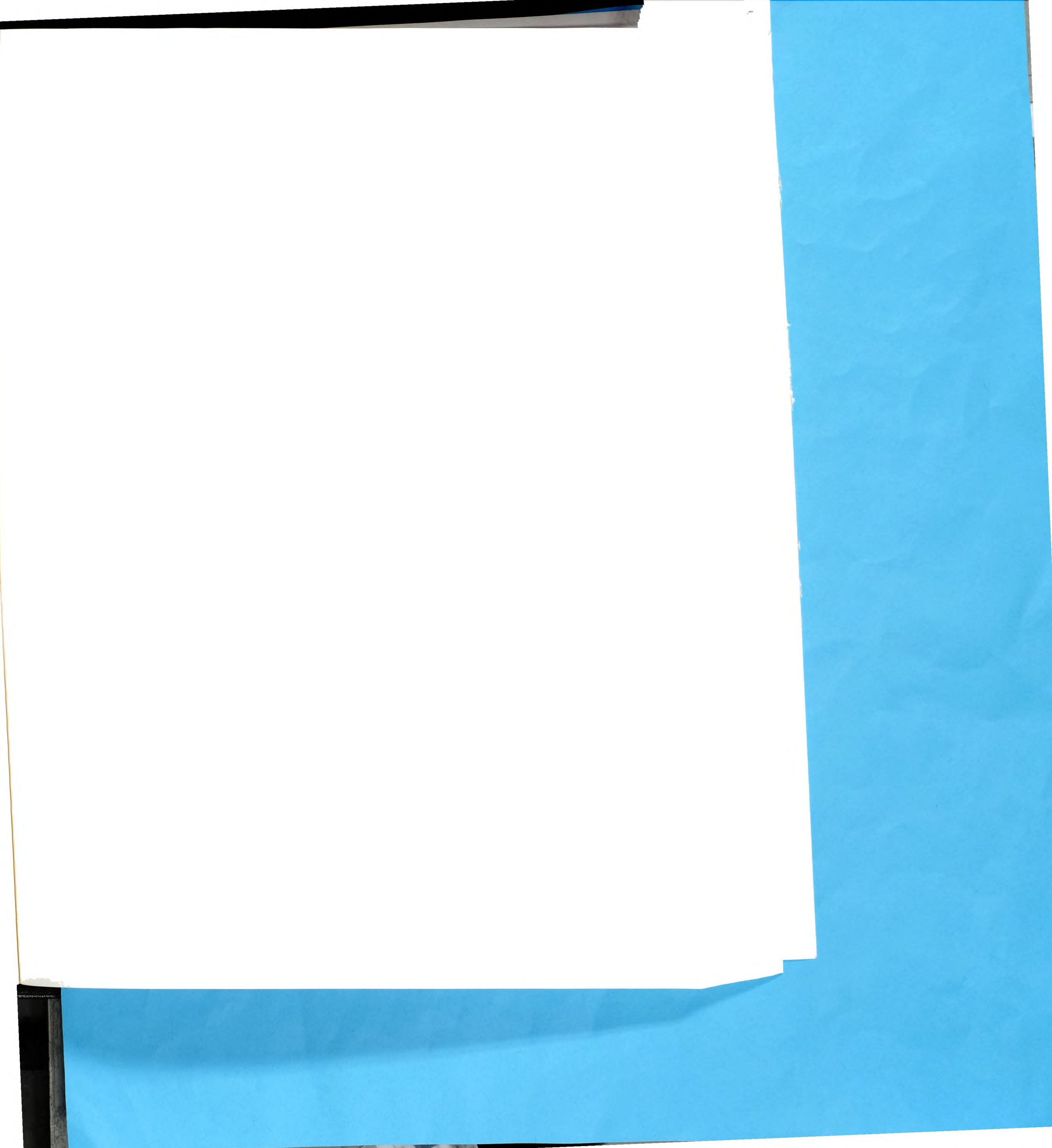

FOV, the image starts to appear distorted around the perimeter. This distortion increases with an increase in the field of view due to the curvature of the collecting lens. Optical distortion must be considered when designing an optical system of this type.

6. The spatial resolution of the image carrier is dependent upon the diameter of the bundle, and the individual fiber element core sizes. Standard image carriers cannot resolve objects smaller than about 15 to 20 μm. When imaging a seeded flow field, the limiting spatial resolution of the fiber bundle will cause the particles to appear hazy, thus making it difficult to distinguish individual particles. For the study of the motored engine when viewing the flow field through the spark plug holder, the particles were as small as 5 μm. In order to resolve these particles, the bundle diameter should be at least 15 mm and the individual fiber core sizes should be 7 μm or smaller.

CHAPTER 5

RECOMMENDATIONS

The observations and ideas discussed in this study represent an introduction to fiber optics as a research tool. Fiber optic technology is continuously improving and it is hoped that this study will provide a foundation for the successful applications of fibers in future studies. A few recommendations for future studies are given below.

1. To use fiber optics as a light delivery system for high power lasers, the coupling of high energy into the fibers needs to be accomplished easily and effectively. Those systems that are successful at coupling high power lasers into single fibers choose a large core fiber and an "isolation room" or "clean room" enclosing the input of the laser light into the fiber. This prevents dust particles from settling on the face of the fiber which causes the reflected laser light to burn the fiber. However, this technique is not easy and the typical transmission efficiency of this system is around 5 to 7%. An alternative solution to coupling high power into a single fiber would be to use a new type of fiber from 3M Company that can withstand power up to 5 GW/cm^2. This type of fiber is called "GLPC" and does not need a clean room for input coupling. However, it has yet to be proven if this technique will be successful.

2. For the problem of coupling high power laser light into fiber bundles, the solution may come in the form of creating a "homemade" bundle with the high power fiber GLPC (this fiber doesn't come in a bundle). However, regardless of the type of fiber used, the epoxies currently manufactured cannot withstand the energy. Research needs to be conducted on developing a material that can secure the fibers together and also transmit the high energy.

3. To create collimated light for the output of fibers, small collimating lenses must be used. However, the smaller lenses introduce more aberrations because of the difficulty in machining and polishing accurately. These aberration may be corrected be constructing an achromatic lens, which is actually two lenses cemented together. For ultra-violet light, an achromatic lens can also be used, but it must be a UV grade quartz lens. These are not standard, but they can be manufactured.

4. When using image carriers for flow visualization, light transmitting ability and field of view (FOV) are two important factors to consider. An 80 degree FOV is wide enough to capture most of the flow field area, though a 120 degrees FOV adapter lens would be ideal. For a 120 degree FOV, the image carrier should have an image transmitting diameter of about 25 mm. The number of fibers is dependent on the core size, but a smaller core produces better spatial resolution. An 80 degree FOV should have an imaging diameter of about 20 mm. These relationships are based on the reduction of perimeter distortion and light collecting abilities for the desired FOV.

5. When using microballoons to seed the flow, an analysis should be done to see how well the microballoons follow the flow. This could be done by conducting a comparison study using sub-micron particles and taking LDV measurements and then repeating the test with microballoons to see how the flow changes. Also, there must be a better method developed for measuring the flow rate of the microballoons.

6. For the types of flow visualization studies described in this study, not only are the optical systems important for the success of the study, but careful attention must also be paid to other test parameters as well. Some important parameters are maintaining the high energy of the laser, using optimal collecting lenses in the camera and using particles which have sufficient light scatter and follow the flow accurately.

APPENDIX A

APPENDIX A

The Microballoon Seeder

The flow visualization technique used in these studies has been greatly enhanced by the use of a specially designed particle mixer. This device is designed to completely mix the seed before entering the test area. Before development of the mixer, particles were directed into the flow in small amounts through the intake port. With the new mixing device, particles can be completely mixed and stored in a large reservoir for continuous use during testing. This device also helps to alleviate turbulent flow entering the test site which occurs if particles are added directly into the intake port.

The particles used to seed the flow are phenolic microballoon particles supplied by Union Carbide and designated as BJO-0930 (density of 0.23 g/cm^3). In an earlier study, by Schock et.al [14], it was discovered that these particles showed significant improvement and consistency in visual contrast over other seeding particles such as titanium dioxide or aluminum particles. This improved light scattering ability provided more detail which allowed for a greater understanding of the major flow features.

To prevent agglomeration, the microballoons must be thoroughly dried and mixed with the air stream before entering the test area. This new particle mixing device or seeder was designed to enhance the seeding procedure for flow visualization studies using microballoons. A schematic of the seeder is shown in figure A.1.

In the seeder, the mixing of the microballoons takes place in a 60 liter cylindrical enclosure. Two devices are used to mix the particles once they are dried and placed onto the wire screen in the container. The first device is a fan with a 3000 rpm motor that serves to agitate the microballoons and keep them swirling in the container. The fan is located just bellow the center of the container, therefore, any particles not entrained in

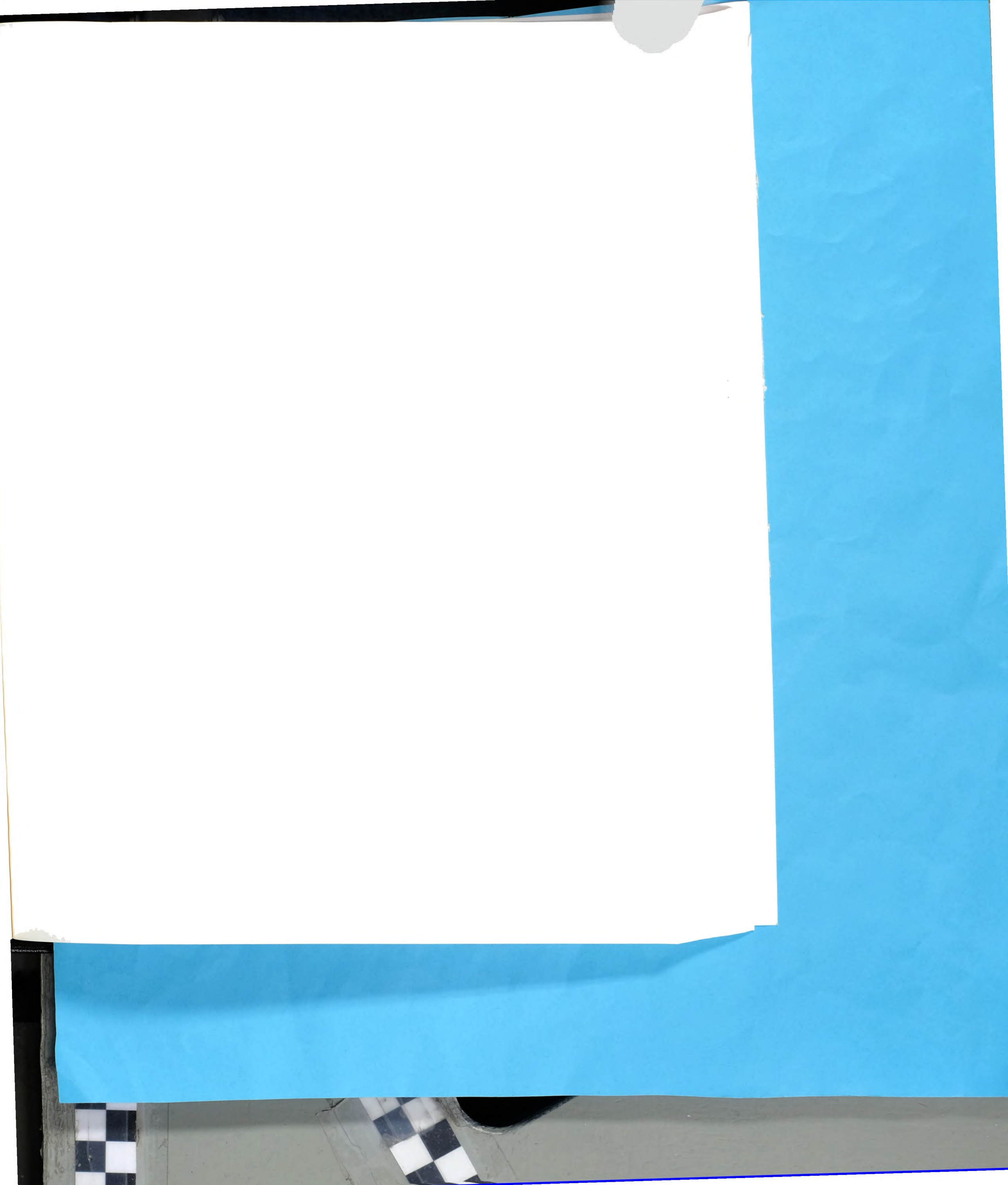

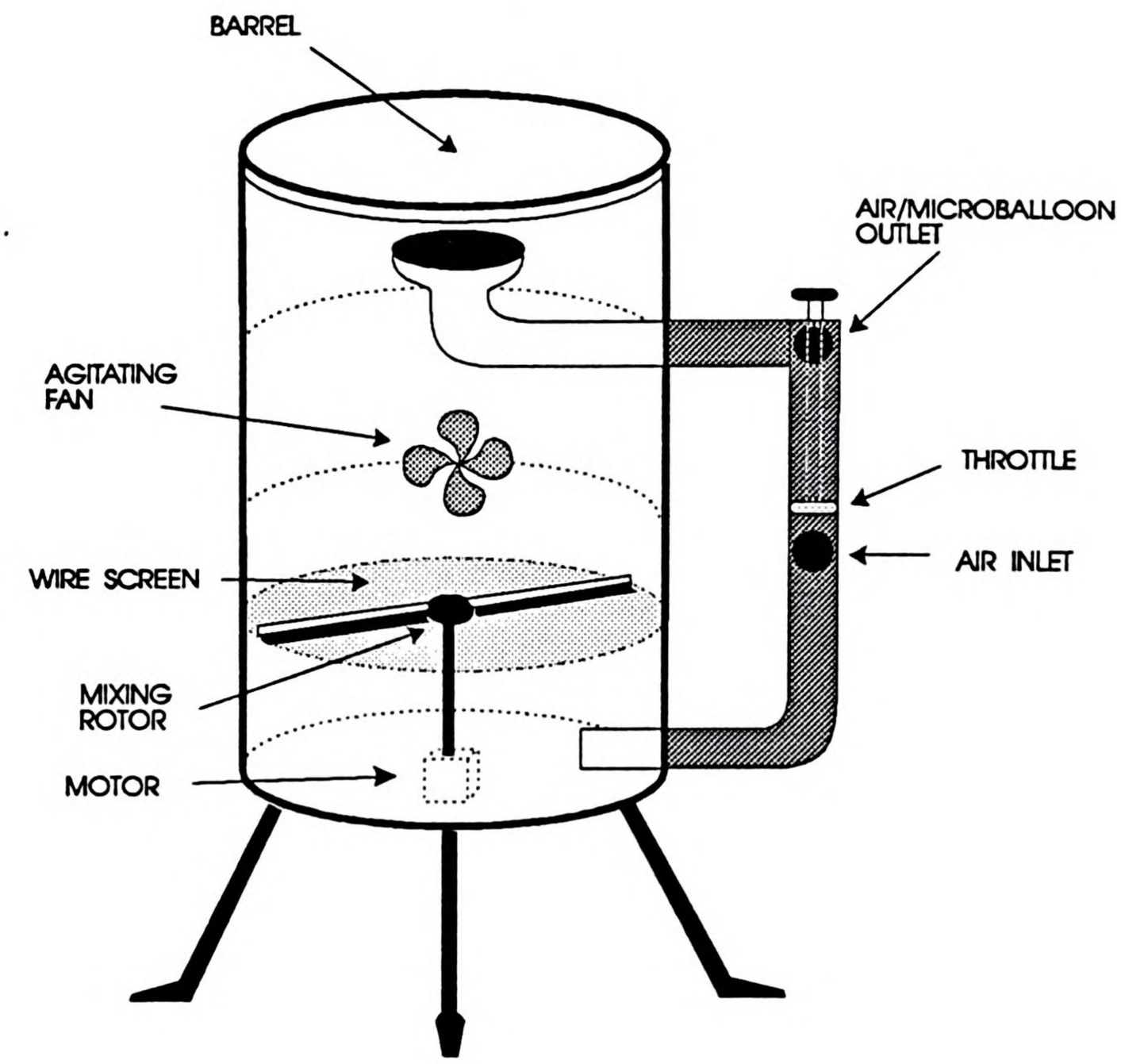

Figure A.1 Schematic of microballoon seeder.

the swirling motion of the fan will fall to a wire screen mesh located about 5 inches below the fan. The screen is 40 x 40 line mesh per inch and the wire diameter is 0.01 inch. This mesh prohibits the clumps of microballoons from falling to the base of the container where the air inlet is located. Just above the mesh sits a two-arm mixer with a 28 rpm gear reduction motor which serves to move and lift any microballoons that settle on the wire screen into the swirling air steams of the fan. Once the inlet air is flowing through the screen, the microballoons are lifted off and tend to hover just above the screen. The rotating arms of the mixer then force the hovering microballoons into the air stream of the fan.

The air inlet and outlet for the seeder is made of 4 inch PVC tubing. The direction of the airflow intake is governed by a throttling valve shown in figure A.2. The

air will bypass the microballoons (cylindrical enclosure) when the throttle is in the down position. The path of the air flow for the throttle in the down position is shown in figure A.2 (a). When the throttle is up, the air is redirected into the cylindrical enclosure and entrains the microballoons. The entrained air containing the microballoons is then sent to the test area through the outlet of the seeder. The outlet was placed at the top of the mixing chamber in order to reduce the amount of heavy microballoon clumps from entering into the airflow. These clumps would tend to hover or swirl in the lower portion of the chamber.

The amount of microballoons sent into the test area, or the density of air to seed can be controlled by a number of methods. The first method deals with the amount of microballoons placed in the seeder. If too many microballoons are used, the flow will be saturated and an accurate representation of the flow field will be masked. The other method used to control the density concerns the position of the throttle. In figure A.2 (c), if the throttle is positioned in the middle of the inlet pipe, the mixture entering the test area will contain pure air and air mixed with microballoons. This mixture of air and microballoons occurs because air travels through both the seeder bypass and the seeder itself. Either one of the above mentioned methods can be used to control particle saturation.

The first step in operating the seeder is to load the microballoons onto the wire screen and seal the lid on the container. The throttle should be in the down position to start with so that only pure air is sent to the test area which completely bypasses the wire screen covered with microballoons. It is important to avoid the entrainment of microballoons through the seeder and into the test area before they are actually needed. The next step is to turn on the agitating fan to stir up the particles. After this step the throttle or flow valve is opened and the mixing rotor is turned on. This ensures that the mixer will push hovering microballoons into the swirling motion of the fan. Once

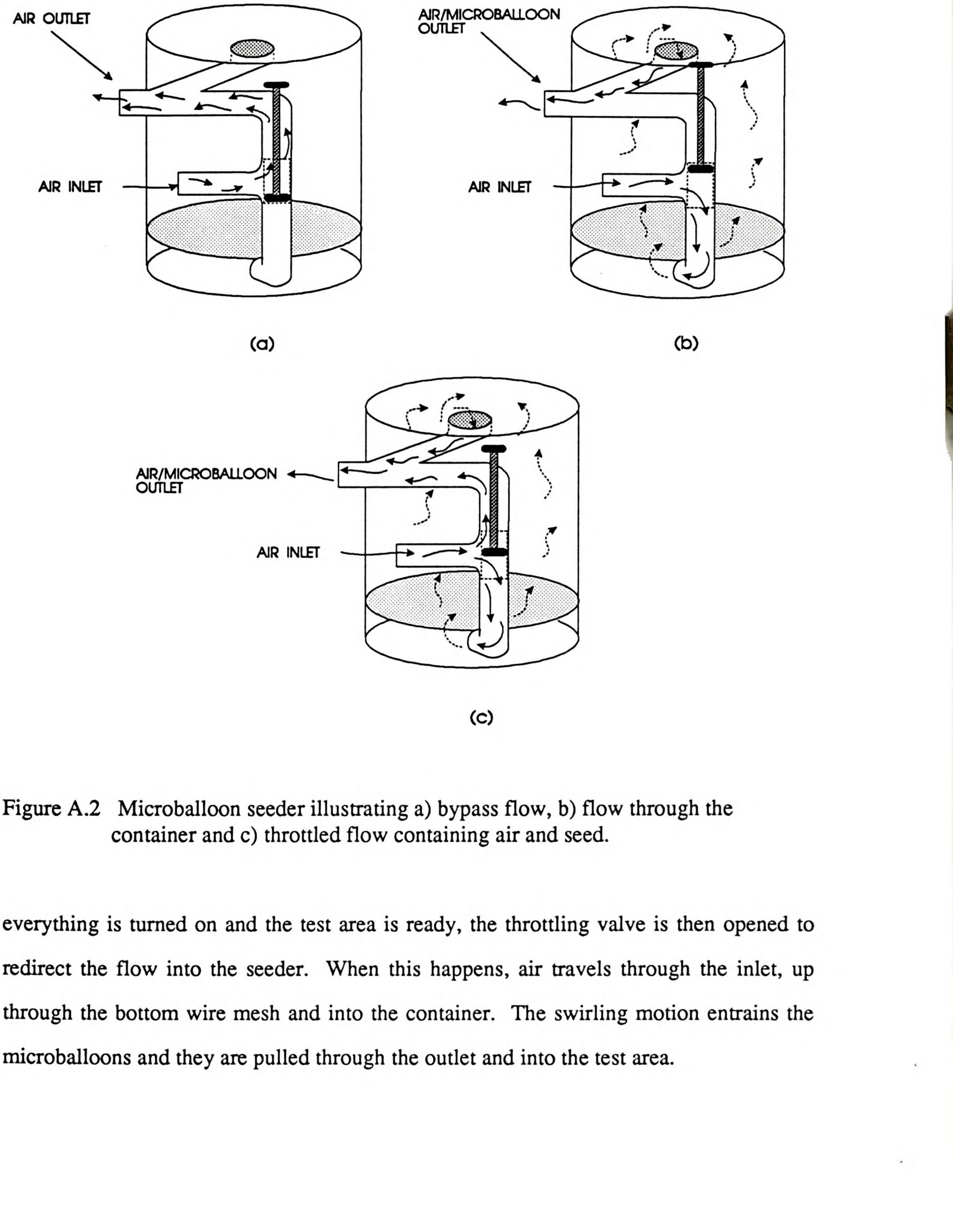

Figure A.2 Microballoon seeder illustrating a) bypass flow, b) flow through the container and c) throttled flow containing air and seed.

everything is turned on and the test area is ready, the throttling valve is then opened to redirect the flow into the seeder. When this happens, air travels through the inlet, up through the bottom wire mesh and into the container. The swirling motion entrains the microballoons and they are pulled through the outlet and into the test area.

APPENDIX B

APPENDIX B

MICROBALLOON CONCENTRATIONS FOR DIFFERENT FLOW RATES

Test 1: Steady State 2.2 Liter Cylinder Head

Comparison of flow rates:

Amount of microballoons initially in seeder:	0.375 gal.
Assume 80% of microballoons went through engine:	0.300 gal.
Depletion of microballoons (time elapsed):	6 sec.

--- Flow rate of microballoons = 0.0067 ft^3/s

--- Flow rate of air through engine = 38 cfm = 0.633 ft^3/s

Microballoons are entrained in the air, and a comparison of flow rates reveals that the seeded air through the engine contains 99.08% air, or approximately 1% seed.

Comparison of density:

Density of microballoons = 230 kg/m^3

Density of air = 1.20 kg/m^3

--- Density of seed and air = 0.99×1.20

$+ 0.01 \times 230$

3.49 kg/m^3

When comparing the seed and air mixture density to the density of air, the seeded mixture increases the density of the flow field by 291%.

Test 2: Motored 3.5 Liter Engine

Comparison of flow rates:

Amount of microballoons initially in seeder:	0.125 gal.
Assume 80% of microballoons went through engine:	0.100 gal.
Depletion of microballoons (time elapsed):	5 sec.

--- Flow rate of microballoons = 0.0027 ft^3/s

--- Flow rate of air through engine = 9 cfm = 0.15 ft^3/s

Microballoons are entrained in the air, and a comparison of flow rates reveals that the seeded air through the engine contains 98.2% air, or approximately 1.8% seed.

Comparison of density:

Density of microballoons = 230 kg/m^3

Density of air = 1.20 kg/m^3

--- Density of seed and air = 0.982×1.20

$+ 0.018 \times 230$

5.32 kg/m^3

When comparing the seed and air mixture density to the density of air, the seeded mixture increases the density of the flow field by 443%.

It should be noted that these calculations are dependent upon the time it takes for the microballoons to exit the seeder. This factor is very hard to measure because the swirling motion of the seed makes it difficult to tell when all the seed has exited the seeder. When doing further calculations, an accurate method of timing the departure of the microballoons from the seeder should be developed.

LIST OF REFERENCES

1. H.S. Hilbert and R.E. Falco, "Measurements of Flows During Scavenging in a Two Stroke Engine," SAE Paper 910671, 1991.

2. D.L. Reuss, R.J. Adrian, C.C. Landreth, D.T. French and T.D. Fansler, "Instantaneous Planar Measurements of Velocity and Large-Scale Vorticity and Strain Rate in an Engine Using Particle-Image Velocimetry," SAE Paper 890616, 1989.

3. F. Hamady, T. Stucken and H. Schock, "Airflow Visualization and LDV Measurements in a Motored Rotary Engine Assembly Part I: Flow Visualization," SAE Paper 900030, 1990.

4. S.L. Kaufman, "Fiber Optics in Laser Doppler Velocimetry," Laser & Applications July 1986, pp. 71-73.

5. M.G. Jones, "New Lenses Expand the Use of High-Power Lasers," Tooling & Production-Advanced Laser Technology, 1984.

6. K.H. Schonborn and W. Wodrich, "Handling and Safety Aspects of Fiber Optic Laser Beam Delivery Systems," SPIE Vol. 906 Optical Fibers in Medicine III, 1988, pp. 251-253.

7. G. Stareev, B. Mroziewicz, S. Banasiak and E. Dobosz, "High Power Pulse Lasers for Fiber Optic Measurements," SPIE Vol. 670 Optical Fibers and Their Applications IV, 1986, pp. 60-65.

8. E. A. Lacy, Fiber Optics , Prentice-Hall, Englewood Cliffs, NJ, 1982.

9. S. Geckeler, Optical Fiber Transmission Systems, Artech House, Norwood, MA 1987, pp 16-18.

10. "Selfoc Fiber Collimators Brochure", NSG America Inc., Somerset, NJ, 1988.

11. "Image Carrier Operation Manual", Olympus Corporation, Lake Success, NY, 1988.

12. "Fiber Optics: Theory and Applications Technical Memorandum", Galileo Electro-optics Corporation, Sturbridge, MA, 1989.

13 T. Morita, F. Hamady, T. Stuecken, C. Somerton and H. Schock, "Fuel-Air Mixture Visualization in a Motored Rotary Engine Assembly," SAE Paper 910704, 1991.

14. H. Schock, F. Hamady, M. DeFilippis, T. Stuecken, C. Gendrich and L.A. LaPoint, "High Frame Rate Flow Visualization and LDV Measurements in a Steady State Flow Cylinder Head Assembly," SAE Paper 910473, 1991.

15. M. Born and E. Wolf, Principles of Optics, Pergamon Press, Oxford, England, 1970, pp. 653-655.

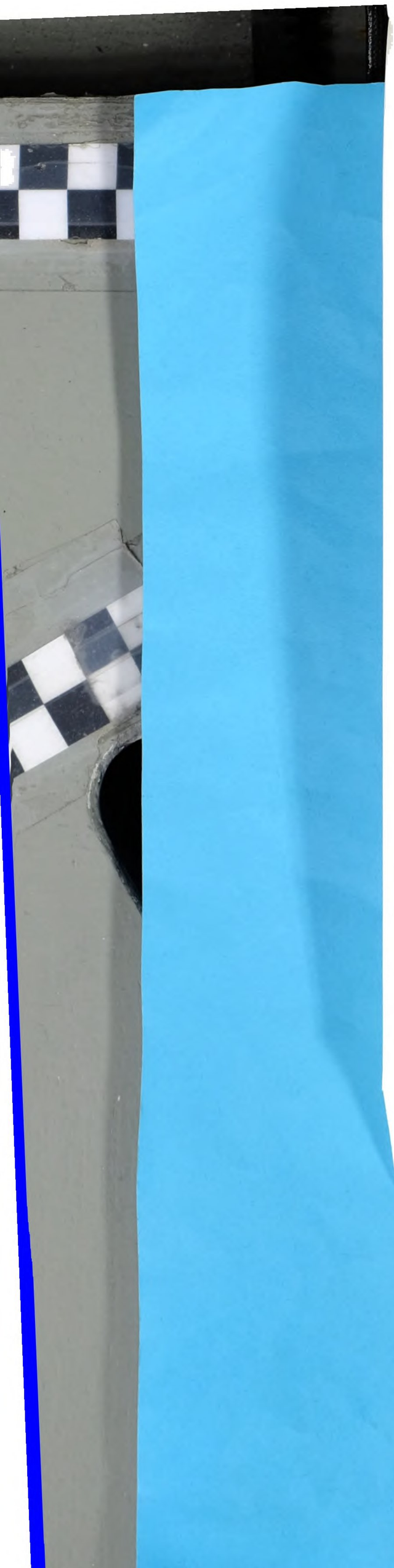

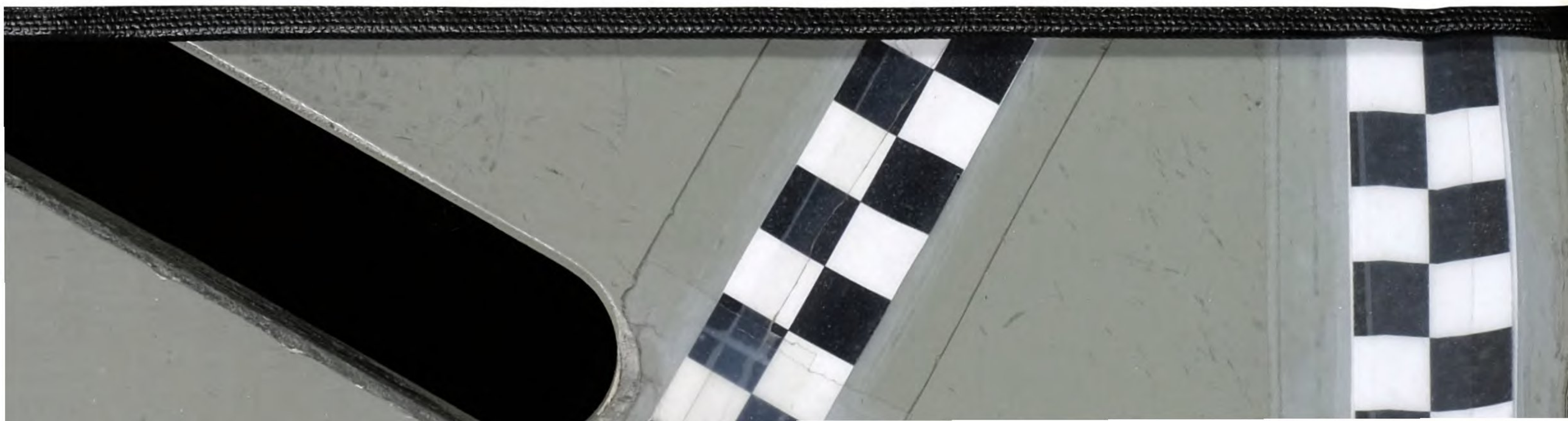

MICHIGAN STATE UNIV. LIBRARIES
31293008969689